Acta Pharmaceutica Sinica B 2024;14(10):4526–4543

Chinese Pharmaceutical Association
Institute of Materia Medica, Chinese Academy of Medical Sciences

Acta Pharmaceutica Sinica B

www.elsevier.com/locate/apsb
www.sciencedirect.com

ORIGINAL ARTICLE

Disease-derived circulating extracellular vesicle preconditioning: A promising strategy for precision mesenchymal stem cell therapy

Ke Lv[a], Tian Wu[a], Shuyun Liu[a], Peng Lou[a], Pingya Zhou[a], Yizhuo Wang[a], Xiyue Zhou[a], Shu Zhang[b], Dan Du[c], Yanrong Lu[a], Meihua Wan[d,e,*], Jingping Liu[a,*]

[a]*Department of Integrated Traditional Chinese and Western Medicine and NHC Key Laboratory of Transplant Engineering and Immunology, Frontiers Science Center for Disease-related Molecular Network, West China Hospital, Sichuan University, Chengdu 610041, China*
[b]*Department of Emergency Medicine, Emergency Medical Laboratory, West China Hospital, Sichuan University, Chengdu 610041, China*
[c]*Advanced Mass Spectrometry Center, Research Core Facility, Frontiers Science Center for Disease-related Molecular Network, West China Hospital, Sichuan University, Chengdu 610041, China*
[d]*West China Center of Excellence for Pancreatitis, Institute of Integrated Traditional Chinese and Western Medicine, West China Hospital, Sichuan University, Chengdu 610041, China*
[e]*The First People's Hospital of Shuangliu District, Chengdu 610299, China*

Received 18 March 2024; received in revised form 18 June 2024; accepted 19 June 2024

KEY WORDS

Regenerative medicine;
Mesenchymal stem cell;
Circulating extracellular vesicle;
Tissue injury;
Metabolic reprogramming;
Inflammation;
Cell death;
Preconditioning

Abstract Mesenchymal stem cell (MSC)-based therapies have emerged as promising methods for regenerative medicine; however, how to precisely enhance their tissue repair effects is still a major question in the field. Circulating extracellular vesicles (EVs) from diseased states carry diverse pathological information and affect the functions of recipient cells. Based on this unique property, we report that disease-derived circulating EV (disease-EV) preconditioning is a potent strategy for precisely enhancing the tissue repair potency of MSCs in diverse disease models. Briefly, plasma EVs from lung or kidney tissue injuries were shown to contain distinctly enriched molecules and were shown to induce tissue injury-specific gene expression responses in cultured MSCs. Disease-EV preconditioning improved the performance (including proliferation, migration, and growth factor production) of MSCs through metabolic reprogramming (such as *via* enhanced oxidative phosphorylation and lipid metabolism) without inducing an adverse immune response. Consequently, compared with normal MSCs, disease-

*Corresponding authors.
E-mail addresses: liujingping@scu.edu.cn (Jingping Liu), wanmh@scu.edu.cn (Meihua Wan).

Peer review under the responsibility of Chinese Pharmaceutical Association and Institute of Materia Medica, Chinese Academy of Medical Sciences.

https://doi.org/10.1016/j.apsb.2024.06.027

EV-preconditioned MSCs exhibited superior tissue repair effects (including anti-inflammatory and anti-apoptotic effects) in diverse types of tissue injury (such as acute lung or kidney injury). Disease-derived EVs may serve as a type of "off-the-shelf" product due to multiple advantages, such as flexibility, stability, long-term storage, and ease of shipment and use. This study highlights the idea that disease-EV preconditioning is a robust strategy for precisely enhancing the regenerative capacity of MSC-based therapies.

1. Introduction

Mesenchymal stem cell (MSC)-based therapies have emerged as promising methods for treating various forms of tissue injury[1,2]. Increasing evidence indicates that MSC therapies can mainly promote tissue repair by exerting immunomodulatory, pro-angiogenic, or antiapoptotic effects through paracrine mechanisms[2]. For example, intravenously injected (IV) MSCs attenuated acute lung injury (ALI) and acute kidney injury (AKI) by reducing inflammation and cell apoptosis in preclinical models[3,4]. However, the therapeutic outcomes of MSCs in clinical trials remain unsatisfactory; moreover, in certain studies, MSC treatments are reported to have moderate or even poor efficacy[5,6]. One of the major reasons for these effects is that the viability and bioactivity of MSCs are largely affected by their donor state and *in vitro* culture conditions, while unsatisfactory culture conditions may impair MSC biofunctions, such as proliferation, migration, and paracrine effects[7]. Therefore, novel strategies to enhance the tissue repair potency of MSC-based therapies are urgently needed.

Increasing evidence indicates that MSCs have a 'short-term-memory' effect in response to microenvironmental stimuli *in vitro*, thus avoiding the need for *in vivo* activation of MSCs when aiming toward enhanced therapeutic effects[6]. To mimic the disease microenvironment where transplanted MSCs are intended to be applied, multiple strategies, such as preconditioning and genetic modifications of MSCs, have been extensively reported[1,5,6]. For example, *in vitro*, preconditioning of MSCs with individual pathological factors, such as hypoxia, cytokines, and physical stress, may activate certain signaling pathways to counter the harsh microenvironment of the injured tissue sites, thus partially improving the survival, homing ability, or paracrine effects of the transplanted MSCs *in vivo*[1]. However, these single factors (such as hypoxia and cytokines) are not disease-specific and cannot accurately represent the complications of disease in cultured MSCs *in vitro*. Therefore, to precisely enhance the tissue repair potency of MSC-based therapies, additional disease-specific preconditioning strategies are needed.

Extracellular vesicles (EVs) are small lipid membrane vesicles (~50−1000 nm) secreted by live cells that are widely distributed in various types of body fluids, such as blood, saliva, and urine[8−10]. It has been well-documented that EVs can act as critical messengers of cell−cell or organ−organ communication by transferring diverse types of biomolecules (such as proteins, lipids, nucleic acids, and metabolites), and the bilayer lipid membrane structure of EVs can protect such biomolecules against enzymatic degradation *in vivo*[8,9]. Moreover, large numbers of EVs can be readily isolated from body fluid samples (such as the blood and urine) of patients who undergo minimally invasive operations. Due to these unique properties, circulating EVs from diseased states have been proposed to be potent biomarkers of various types of diseases due to the fact that they carry diverse disease-specific information from injured tissues or cells[9,11]. For example, circulating EVs from the serum of lipopolysaccharide (LPS)-induced ALI mice could stimulate lung inflammation-related responses *in vivo* and *in vitro*[12]. In contrast, removal of EVs from plasma samples of acute pancreatitis patients significantly decreased macrophage cytokine release compared to that in plasma EVs[13]. Taken together, these findings suggest that circulating EVs carry vital disease-related information and may thereby serve as preconditioning factors for MSCs; however, the detailed and underlying mechanisms involved in these effects have not been previously explored.

Here, we report that disease-derived circulating EV (disease-EV) preconditioning is an efficient strategy for precisely enhancing the tissue repair potency of MSCs in diverse disease models. In brief, compared with those of healthy controls, circulating EVs isolated from the plasma of patients with different diseases have distinct biomolecules, and these EVs can induce specific tissue injury-related gene expression in MSCs. Moreover, disease-EV preconditioning increased the proliferation, migration, and growth factor production of MSCs *via* systemic metabolic rewiring. As a result, compared with normal MSCs, MSCs primed with disease-derived EVs showed superior tissue repair effects on diverse types of tissue injury (Fig. 1). This study suggested that circulating EVs can induce disease-related responses and enhance the performance of MSCs, as well as the fact that disease-EV preconditioning is a potent strategy for precise MSC therapy.

2. Materials and methods

2.1. Identification of disease-related molecules in circulating EVs

The miRNA sequencing data of plasma EV samples from ARDS patients and the proteome assay data of serum EV samples from DKD patients were obtained from previously published studies[14,15]. For analysis of the miRNA profiles of the EVs from ARDS patients, the differentially expressed miRNAs (those with a fold change [FC] > 1.2 and P value < 0.05) were considered significant. Prediction of target genes for miRNAs was conducted using multiMiR (version 1.4.0)[16]. Furthermore, Kyoto Encyclopedia of Genes and Genomes (KEGG) data for the target genes were analyzed using ClusterProfiler[17]. For analysis of the protein profiles of EVs from DKD patients, the differentially expressed proteins (DEPs; FC > 1.2 and P value < 0.05) were considered

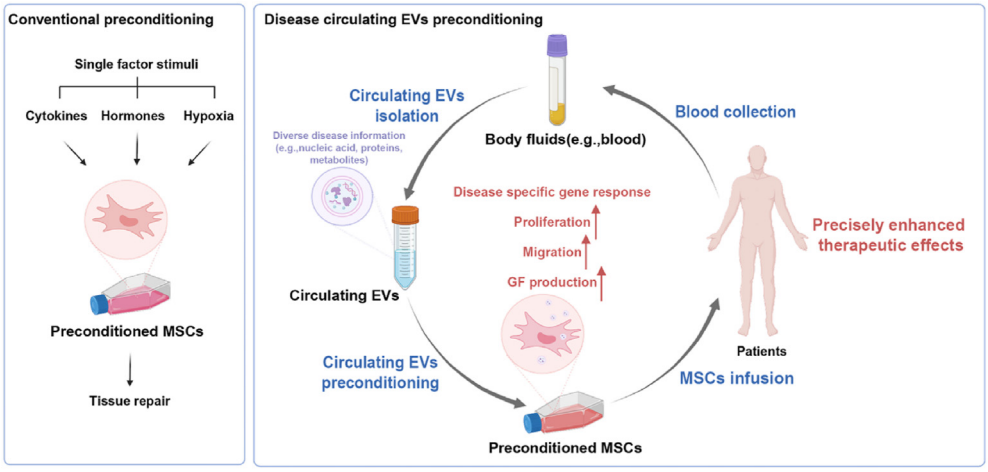

Figure 1 Comparison of the conventional preconditioning strategy and the circulating disease-related EV preconditioning strategy. The conventional preconditioning strategy uses a single factor (*e.g.*, cytokines, hormones, or hypoxia) to prime MSCs but lacks disease specificity. A novel preconditioning strategy was proposed. Disease-derived circulating EVs from body fluids (*e.g.*, blood) can deliver disease information to MSCs when they are preconditioned with MSCs for precisely enhanced therapeutic effects.

significant. ClusterProfiler software (version 4.8.1) was used to analyze the functional enrichment of DEPs, including KEGG pathway enrichment[17]. The visualized results from PCA, volcano plots, heatmaps, KEGG, etc., were obtained using ggplot2 (version 3.4.4) in the R script (version 4.2.3, https://cran.r-project.org/).

2.2. *Collection of plasma samples from AKI model rats*

All animal experiments were conducted according to the National Institutes of Health (NIH) guidelines and approved by the Animal Care and Use Committee of West China Hospital, Sichuan University (Permit No. 20220209007). Animals were housed in individual cages with controlled temperature and humidity and a 12-h cycle of light and dark and were fed standard chow and tap water *ad libitum*. Male Sprague−Dawley rats (180−220 g) were randomly divided into two groups ($n = 20$ per group): the normal control group and the AKI group. Cisplatin (5 mg/mL; MedChemExpress, MCE, HY-17394, New Jersey, USA) was dissolved in normal saline solution (0.9% sodium chloride, *w/v*), and a rat AKI model was induced by IP injection of cisplatin at a dosage of 5 mg/kg body weight, while rats in the normal control group received an equal volume of 0.9% saline solution. On Day two after AKI, the rats were anesthetized, and blood samples were collected after the addition of an anticoagulant (K_2-ethylene diamine tetraacetic acid, K_2-EDTA). Plasma samples were obtained from whole blood using centrifugation (3000 rpm for 15 min at room temperature, Thermo Fisher, ST16R, Waltham, MA, USA).

2.3. *Plasma sample collection from ALI patients*

This study was carried out in accordance with the standards of good clinical practice and the international ethical principles applicable to medical research in humans (Declaration of Helsinki)[18]. A prospective study was performed among patients in the Department of Emergency Medicine of West China Hospital of Sichuan University from August 2022 to August 2023; the study was approved by the Ethics Committee of Biomedical Research. Written informed consent was obtained from all participating people. Informed consent was signed by the patients or their legally authorized representatives when they were mechanically ventilated. A total of 20 consecutive patients with ALI were included. The exclusion criteria included age <18 years, pregnancy, primary coagulation abnormalities, fibrinolytic therapy, immunosuppression due to medication or disease, and hemodialysis. Patients with ALI met the following consensus definitions: the presence of a risk factor (such as sepsis, aspiration, shock, or multiple transfusions), acute onset of bilateral infiltrates on chest radiography, severe hypoxemia with a ratio of arterial oxygen partial pressure and an inspiratory oxygen fraction (PO_2/FiO_2) < 300 for ALI[19]. Plasma samples were isolated from EDTA-pretreated blood samples drawn from the patient's veins by centrifugation at 3000 rpm for 15 min at room temperature.

2.4. *Isolation of circulating EVs from plasma samples*

Circulating EVs were isolated from plasma samples of AKI rats or ALI patients using an ultracentrifugation method as previously described[20]. In brief, plasma samples were centrifuged at 2000×*g* (Thermo Fisher) for 20 min and 10,000×*g* (Avanti JXN-26, Beckman Coulter, Brea, CA, USA) for 30 min at 4 °C to remove platelets and cell debris. EVs were isolated by ultracentrifugation at 120,000×*g* for 70 min at 4 °C on an Optima XPN-100 ultracentrifuge with an SW32Ti rotor (Optima XPN-100, Beckman Coulter). Then, the isolated crude EVs were washed with PBS and subjected to secondary ultracentrifugation (110,000×*g* for 90 min at 4 °C). The purified EV pellets were resuspended in PBS and stored at −80 °C. The protein concentrations of the EVs were quantified using a Bradford assay kit (Thermo Fisher, A55864).

2.5. *Characterization of plasma EVs*

The characterization of EV properties (microstructure, size, and protein markers) was performed according to minimal information available from studies of extracellular vesicles[21]. The microstructure of the EVs was observed using a transmission electron microscope (TEM, Hitachi, H-600, Tokyo, Japan). Briefly, 40 μL of diluted EV sample solution was placed on a carbon-coated

copper grid. After washing with Milli-Q water (Millipore, Advantage A10, Sigma, Louis, MO, USA), the EV sample-loaded grid was negatively stained with 2% phosphotungstic acid solution. After air-drying at room temperature, the grid was observed *via* TEM at a voltage of 80 kV. The diameter of the EVs was analyzed by ImageJ software (NIH, Bethesda, MD, USA) in one hundred forty biological replicates of each group.

The size distribution of the EV samples was measured using nano tracking analysis (NTA) on a Zeta View PMX 120 (Particle Metrix, Meerbusch, Germany) as previously described[22]. Briefly, EV samples were diluted (*v*/*v*, 1:3000) with Milli-Q water, and their size distributions and particle concentrations were analyzed using the parameters (min area 5, max area 1000, min brightness 20, and camera 0.713 μm/px) at 25 °C. The mean particle size of each EV type was calculated by averaging the median particle size of three biological replicates of each group.

The protein markers of the EV samples were detected using western blotting with anti-HSP70 (ABClonal, A0284, Wuhan, China), anti-TSG101 (Proteintech, 67381-1-IG, Rosemont, IL, USA), anti-GM130 (Cell Signaling Technology, CST, 12480, Beverly, MA, USA), anti-CD63 (Abcam, ab134045, Cambridge, UK), anti-CD9 (SAB, 40708, Maryland, USA), or anti-Calnexin (CST, 2433) as previously reported[22].

2.6. Western blotting

Cell or tissue samples were lysed in radioimmunoprecipitation assay buffer (RIPA buffer; CWBIO, CW2333S, Beijing, China), and protein concentrations were determined using a BCA assay kit (Thermo Fisher, A55864). Equal amounts of proteins were electrophoresed on 12.5% sodium dodecyl sulfate-polyacrylamide gels (SDS−PAGE) and then transferred to polyvinylidene difluoride membranes (PVDF, Millipore, USA). The PVDF membrane was blocked in 5% nonfat milk buffer and then incubated with primary antibodies, including anti-GM130, anti-TSG101, anti-HSP70, anti-CD63, anti-CD9, and anti-Calnexin, at 4 °C overnight. After washing with PBST, the PVDF membrane was incubated with the corresponding HRP-conjugated secondary antibodies (ZSGB-Bio, ZB-2301, ZB-2305, Beijing, China) at 37 °C for 1 h. The bands on the PVDF membrane were visualized with an enhanced chemiluminescence (ECL) kit (MCE, HY-K1005).

2.7. Cellular uptake assay of plasma EVs

The plasma EVs were labeled with MemGlow (Cytoskeleton, MG02-02, DENVER, CO, USA) according to the manufacturer's protocol. Macrophages (2×10^5 cells) or MSCs (1×10^5 cells) were incubated with MemGlow-labeled EVs (10 μg/mL) for 4 h at 37 °C with 5% CO_2. After incubation, the cells were washed with PBS and fixed in 10% formaldehyde at room temperature for 10 min, followed by staining with FITC-phalloidin (Yeasen Biotechnology, 40735ES, Shanghai, China) and 4′,6-diamino-2-phenylindole (DAPI, Sigma, 10236276001) according to the manufacturer's instructions. The stained cells were observed by an inverted fluorescence microscope (Zeiss, Imager Z2, Oberkochen, Germany).

2.8. Macrophage culture and plasma EV treatments

Primary mouse macrophages were isolated from the bone marrow of male C57BL/6 mice (6 weeks old) as previously reported[22]. The macrophages were cultured in RPMI 1640 medium (Gibco, 31870082, Grand Island, NY, USA) supplemented with 10% heat-inactivated FBS (Capricorn Scientific GmbH, FBS-11A, Ebersdorferglund, Hesse, Germany), 1% penicillin/streptomycin and recombinant mouse macrophage colony-stimulating factor (mM-CSF, 20 ng/mL; Novoprotein, CB34, Suzhou, China). Macrophages (2×10^5 cells) were treated with plasma EVs (10 μg/mL) or EV-free supernatant (10 μg/mL) for 4 h at 37 °C, after which the cells were collected. The gene expression of cytokines (*Il-1β*, *Il-6*, and *Tnf-α*) and chemokines (*Mcp-1*) in macrophages was detected using qPCR according to previous methods.

2.9. Quantitative real-time polymerase chain reaction (qPCR)

Total RNA was extracted from cells using TRIzol (Gibco, 15596018CN) and reverse transcribed into cDNA using a HiScriptQ RT SuperMix for qPCR Kit (Vazyme Biotech, R123-01, Nanjing, China). The primers used in this study are listed in Supporting Information Table S1. Polymerase chain reaction (PCR) was performed using SYBR Green PCR mix (Vazyme Biotech, Q131-02/03) in a real-time PCR detection system (Bio-Rad, S1000, Hercules, CA, USA). The data were analyzed using Bio-Rad CFX Manager software, and relative changes in mRNA levels were calculated by the delta-delta Ct method with the S18 ribosomal protein (*Rps18*) serving as the internal reference gene as previously described[22].

2.10. MSC culture and plasma EV preconditioning

Primary human umbilical cord MSCs were obtained from Sichuan Neo-life Stem Cell Biotech & Sichuan Stem Cell Bank (Chengdu, China). MSCs were cultured in DMEM (Gibco, 11885092) supplemented with 10% FBS (Capricorn Scientific GmbH) and 1% penicillin/streptomycin (Gibco) at 37 °C with 5% CO_2. Preconditioning experiments were performed on MSCs at passages 3−5. In brief, MSCs were incubated with plasma EVs (10 μg/mL) from ALI patients or AKI rats at 37 °C for 12 h, and then the preconditioned MSCs were washed with PBS and collected for further experiments.

2.11. mRNA sequencing analysis of MSCs

Total RNA was extracted from MSCs with or without EV preconditioning using TRIzol and then treated with DNase I (Takara, Shiga, Japan) to deplete the genomic DNA according to the manufacturer's instructions. High-quality RNA was quantified with a 2100 Bioanalyzer (Agilent, Santa Clara, CA, USA), and the RNA was quantified with an ND-2000 (NanoDrop Technologies, Wilmington, DE, USA) to construct a sequencing library. The RNA sequencing transcriptome library was prepared following the instructions of the TruSeqTM RNA Sample Preparation Kit from Illumina (San Diego, CA, USA). cDNA was synthesized using a SuperScript double-stranded cDNA Synthesis Kit (Invitrogen, Grand Island, NY, USA) with random hexamer primers (Illumina). Libraries were size selected for cDNA target fragments of 300 bp on 2% low-range Ultra agarose followed by PCR amplification using Phusion DNA polymerase (New England Biolabs, Ipswich, MA, USA). The expression abundance of each gene was determined using TPM, and the DEGs were identified using DESeq2 based on read counts. Subsequently, clusterProfiler (version 4.8.1) was used to analyze the functional enrichment of the DEGs (FC $>$ 1.2 and P value $<$ 0.05), including GO pathway

enrichment[17], to elucidate the functions and pathways of these genes in biological processes. Finally, ggplot2 (version 3.4.4) was used to visualize the analysis results, such as by generating heatmaps and volcano plots in the R script (version 4.2.3).

2.12. *miRNA sequencing analysis of MSCs*

Total RNA was extracted from MSCs with or without EV preconditioning using TRIzol and then treated with DNase I to deplete the genomic DNA. High-quality RNA was quantified with a 2100 Bioanalyzer (Agilent), and the RNA was quantified with an ND-2000 to construct a sequencing library. Sequencing libraries were generated using a QIAseq MiNRA Library Kit (Qiagen) following the manufacturer's protocol. The activated 5′ and 3′ adaptors were ligated to the total RNA. Then, the adaptor-ligated RNA was transcribed into first-strand cDNA by using reverse transcriptase and random primers. PCR was performed using primers complementary for 11−12 cycles, and fragments of appropriate size were isolated *via* a 6% Novex TBE PAGE gel. After quantification by Qubit4.0, the single-end RNA-seq library was sequenced with an Illumina NovaSeq X Plus sequencer.

All identical sequences with sizes of 18 to 32 nt were counted and removed from the initial dataset. After the elimination of nonmiRNAs (rRNA, tRNA, snoRNA, etc.), the expression of miRNAs was analyzed using perfectly matched sequences from the BLAST search of miRbase (V22, http://www.mirbase.org/). Differentially expressed miRNAs (FC $>$ 1.2 and P value $<$ 0.05) were considered significant. Prediction of target genes for miRNAs was conducted using multiMiR (version 1.4.0)[16]. Furthermore, the KEGG data of the target genes were analyzed using ClusterProfiler (version 4.8.1)[17]. The visualized results from PCA, volcano plots, heatmaps, Venn diagrams, KEGG, etc., were obtained using ggplot2 (version 3.4.4) in the R script (version 4.2.3).

2.13. *MSC proliferation assay*

The proliferation rates of MSCs with or without EV preconditioning were assessed using a cell counting kit-8 (CCK-8) assay (Dojindo, CK04, Kyushu Island, Japan) according to the manufacturer's protocol. Briefly, MSCs (5×10^3 cells) were seeded into a 96-well plate and then treated with plasma EVs (10 μg/mL), plasma EVs plus an SCD1 inhibitor (50 nmol/L; MCE, HY-141525) or FCCP (500 nmol/L; Sigma, C2920) for 24 h. The absorbance at 450 nm in each well of the plate was measured using a microplate reader (BioTek, SYNERGY H1, Winooski, Vermont, USA), and the relative cell proliferation rates were calculated as Eq. (1):

$$\text{Proliferation ratio} = (A_1 - A_0)/\overline{A}_C \quad (1)$$

where A_1 represents the absorbance in each well, A_0 represents the absorbance in the blank well, and $\overline{A}_C$ represents the average absorbance in the control wells.

2.14. *MSC migration assay*

The cell migration rates of MSCs were assessed using a scratch test. MSCs (1.5×10^4 cells) were plated into the wells of 96-well plates and incubated to reach confluence. The cell monolayer was scratched using a pipette tip and washed with PBS to remove detached cells. MSCs were then cultured in serum-free medium supplemented with or without plasma EVs (10 μg/mL), plasma EVs (10 μg/mL) plus an SCD1 inhibitor (50 nmol/L; MCE) or FCCP (500 nmol/L; Sigma). The plates were photographed every 6 h by an IncuCyte SX5 (Sartorius, 4816, Göttingen, Germany). The relative migration rates of the MSCs were calculated as Eq. (2):

$$\text{Migration rate } (\%) = (A_0 - A_n)/A_0 \times 100 \quad (2)$$

where A_0 represents the area of the initial wound area, and A_n represents the remaining area of the wound at the metering point.

2.15. *MSC growth factor production*

Briefly, MSCs (1×10^5 cells) were seeded into the wells of 12-well plates and then treated with plasma EVs (10 μg/mL), plasma EVs (10 μg/mL), an SCD1 inhibitor (50 nmol/L, MCE) or FCCP (500 nmol/L, Sigma) for 24 h. Total RNA was extracted from the MSCs using TRIzol. The gene expression of growth factors (*KGF*, *HGF*, *FGF2*, and *VEGF*) in MSCs was analyzed using Bio-Rad CFX Manager software.

2.16. *LC−MS/MS-based targeted metabolomics analysis of MSCs*

Targeted MS-based aqueous metabolomics was performed on an Agilent 1260 LC (Agilent) coupled to an AB Sciex Qtrap 5500 MS (AB Sciex, Toronto, Canada) system as described previously[23]. In brief, MSCs (1×10^6 cells) from different conditions were collected and washed with precooled PBS. The metabolites in the aqueous fraction of cells were extracted using 80% spike MeOH/H_2O (8:2, *v/v*) containing internal standards (0.096 mmol/L $^{13}C_6$-glucose and 0.021 mmol/L $^{13}C_2$-glutamic acid) on dry ice for 30 min. After centrifugation (13,000 rpm for 10 min at 4 °C), the supernatant was collected and dried in a SpeedVac (Eppendorf, Hamburg, Germany).

The dried samples were dissolved in 0.5 mL of hydrophilic interaction chromatography (HILIC) solution. After centrifugation (13,000 rpm for 10 min at 4 °C) and filtration (0.22 μm filter; Thermo Scientific), 5 and 15 μL sample aliquots were injected into the LC−MS/MS system under positive and negative ion modes, respectively. A pooled sample was used as the quality control (QC) sample, and the QC sample was injected after every 10 study samples. Chromatographic separations of the samples were performed by HILIC using a BEH amide column (2.1 mm × 100 mm, 1.7 μm, Waters, Milford, MA). The 242 identified metabolites with high confidence levels were selected for further analysis. The significantly changed metabolites (DEMs, FC $>$ 1.2, and VIP $>$ 1) were considered significant. GO analysis of the DEGs and significantly changed metabolites was performed using the online tool MetaboAnalyst (https://www.metaboanalyst.ca/MetaboAnalyst/). The visualized results from PLS-DA, volcano plots, heatmaps, and GO pathways were obtained using the R script (version 4.2.3).

2.17. *LC−MS/MS-based lipidomic analysis of MSCs*

Global MS-based lipidomics was performed using an Agilent 1200 LC system coupled to an Agilent 6520 Q-TOF mass spectrometer as previously reported[23]. MSCs (1×10^6 cells) from the different groups were collected and washed with PBS. A CH_2Cl_2/MeOH solution (2:0.9, *v/v*, 2.9 mL) was added to the cells to quench metabolism. The CH_2Cl_2/MeOH solution contained two

lipid standards (3 μL, SPLASH LipidoMIX™ Internal Standard, Avanti, Alabaster, AL, USA). The mixture was transferred to a glass vial, vortexed, and incubated for 30 min at room temperature. Then, water (1 mL) and CH_2Cl_2 (0.9 mL) were added to the mixture, which was vortexed for 5 s and centrifuged at 2000 rpm for 10 min at 4 °C. The lower organic phase was collected and dried using nitrogen.

The dried sample was reconstituted in 100 μL of ACN/CH_2Cl_2 (1:1 *v*/*v*) and loaded into a glass vial for lipidomic analysis. Five microlitres of each prepared sample for positive ESI ionization and 10 μL for negative ESI ionization were injected into an HSS T3 column (2.1 mm × 100 mm, 1.7 μm, Waters), which was heated to 35 °C. The *m*/*z* scan range was 100−2000, and the acquisition rate was 1.0 spectra/s. Differential lipids (FC > 1.2 and VIP > 1) were considered significant. The visualized results from PLS-DA, volcano plots, heatmaps, etc., were obtained using the R script (version 4.2.3).

2.18. Proinflammatory macrophage model and MSC coculture

The macrophages were cultured in RPMI 1640 medium supplemented with 10% FBS (Capricorn Scientific GmbH), 1% penicillin/streptomycin, and mM-CSF (20 ng/mL). Proinflammatory macrophages (M1) were induced by stimulation with LPS (40 ng/mL; Sigma, L2630) for 4 h. M1 macrophages (2×10^5 cells, lower chamber) were then cocultured with normal MSCs (1×10^5 cells, upper chamber) or ALI-EV-preconditioned MSCs (1×10^5 cells, upper chamber) for 24 h using a Transwell system (Corning, 3412, NY, USA). At least three biological replicates were included in each group. The cells in the lower chambers were harvested, and the gene expression of cytokines (*Il-6, Ifn-γ, and Tnf-α*) in the cells was assayed using qPCR.

2.19. Renal TEC injury model and MSC coculture

Human TECs (HK-2 cells) were maintained in DMEM/F12 (Gibco) supplemented with 10% FBS (Capricorn Scientific GmbH) and 1% penicillin/streptomycin. HK-2 cells were cultured in 6-well plates (1.5×10^5 cells/well) and treated with cisplatin (5 nmol/L, MCE) for 48 h. For MSC treatments, injured HK-2 cells (in the lower chamber) were cocultured with normal MSCs (1×10^5 cells in the upper chamber) or AKI-MSCs (1×10^5 cells in the upper chamber) for 24 h in a Transwell system. At least three biological replicates (*e.g.*, three wells of cells) were included in each group. The cells in the lower chambers were harvested, the mRNA levels of *KIM-1*, *NGAL*, and *BAX* were assayed *via* qPCR, and the expression of NGAL and γ-H2AX was assayed *via* immunofluorescence staining.

2.20. Immunofluorescence (IF) staining

Cells or frozen renal tissue sections were fixed with 10% neutral formaldehyde in PBS for 10 min at room temperature, washed with PBS, and permeabilized with 0.3% Triton X-100 for 10 min. After blocking in 1% BSA for 30 min, the cells were incubated with primary antibodies, including anti-8-OHdG (Santa Cruz Biotechnology, sc-393871, Dallas, TX, USA), anti-γ-H2AX (CST, 9718s), anti-Kim-1 (R&D Systems, AF1817, Minneapolis, MN, USA), and anti-neutrophil gelatinase-associated lipocalin (NGAL, ABclonal, A2092), overnight at 4 °C, followed by incubation with a FITC- or TRITC-conjugated secondary antibody (Life Technologies, A11017, CA, USA) for 1 h at 37 °C. Nuclei were visualized by staining with DAPI for 5 min at room temperature. Digital images were captured using a fluorescence microscope (Nikon, N-STORM & A1, Tokyo, Japan) and quantified with NIH ImageJ software.

2.21. In vivo tracking of transplanted MSCs in mice

MSCs with or without plasma EV preconditioning were labeled with DiD (5 μmol/L, Invitrogen, D7757) as previously reported[24]. DiD-labeled MSCs (10^5 or 5×10^5 cells in 100 μL of PBS) were intravenously or intraperitoneally injected into mice with LPS-induced ALI or cisplatin-induced AKI ($n = 3$). Mice in the control group ($n = 3$) received 100 μL of PBS. At selected time points after injection, the mice were anesthetized, and the organs (heart, lung, spleen, liver, and kidneys) were collected and observed on an IVIS Spectrum optical imaging system (Perkin Elmer, Waltham, MA, USA). The fluorescence intensity of DiD-labeled MSCs was quantified by Analyze 12.0 software (Perkin Elmer).

2.22. Mouse ALI model and MSC treatments

All animal experiments were conducted according to the National Institutes of Health (NIH) guidelines and approved by the Animal Care and Use Committee of West China Hospital, Sichuan University (Permit NO. 20220209007). Animals were housed in individual cages with controlled temperature and humidity and a 12-h cycle of light and dark and were fed standard chow and tap water *ad libitum*. Male BALB/c mice were randomly divided into four groups ($n = 6$ per group): healthy control (Con), ALI, ALI + NC-MSCs treatment, and ALI + ALI-MSCs treatment groups. Mouse ALI was induced by intraperitoneal injection of LPS (10 mg/kg body weight) as previously reported[4]. For MSC treatments, ALI mice were intravenously injected with NC-MSCs or ALI-MSCs (1×10^5 cells in 100 μL of PBS per mouse) 30 min after LPS injection. Mice in the ALI alone group were intravenously injected with 100 μL of PBS. At 24 h after MSC treatment, the lung tissues of the mice were collected and subjected to tissue histological examination and qPCR assays.

2.23. Mouse AKI model and MSC treatments

Male C57BL/6 mice were randomly divided into four groups ($n = 6$ per group): healthy control (Con), AKI, AKI + NC-MSCs treatment, and AKI + AKI-MSCs treatment groups. Mouse AKI was induced by intraperitoneal injection of cisplatin (15 mg/kg body weight). For MSC treatments, AKI mice were intraperitoneally injected with NC-MSCs or AKI-MSCs (5×10^5 cells in 200 μL of PBS per mouse) 30 min after cisplatin injection. Mice in the AKI alone group were intraperitoneally injected with 200 μL of PBS. On Day 2, after the MSC treatments, the serum and kidney tissues of the mice were collected and subjected to clinical biochemical tests, histological examination, and qPCR assays.

2.24. Clinical biochemical tests

The concentrations of kidney function parameters, including blood urea nitrogen (BUN) and creatinine (CREA), in the serum samples of the mice were analyzed on a Cobas 6000 biochemistry

analyzer (Roche Diagnostics, Switzerland) using appropriate commercial kits.

2.25. Histological examination

Lung or kidney tissue samples fixed in 10% formaldehyde were embedded in paraffin and cut into 4 μm-thick sections for hematoxylin and eosin (H&E) staining and immunohistochemistry (IHC) staining. For IHC staining, the tissue sections were deparaffinized in xylene and rehydrated in graded concentrations of ethanol, and antigen retrieval was performed with citrate buffer. After inactivation of endogenous peroxidase with 3% H_2O_2, the sections were blocked with 1% bovine serum albumin (BSA), incubated overnight at 4 °C with diluted primary antibodies, including anti-Ly6G (Servicebio, GB11229, Wuhan, China) and anti-MPO (Servicebio, GB11224), and then stained with horseradish peroxide (HRP)-conjugated secondary antibodies (ABclonal) and 3,3'-diaminobenzidine (DAB) substrates. Digital images of stained sections were captured using an upright microscope (Carl Zeiss, Germany).

2.26. Tissue TUNEL staining

Terminal deoxynucleotidyl transferase dUTP nick end labeling (TUNEL) staining of kidney tissues was performed using a commercial kit (Promega, G3250, Madison, WI, USA) following the manufacturer's protocols, and nuclei were stained with DAPI. The stained sections were observed under a fluorescence microscope (Nikon). The average number of $TUNEL^+$ cells in 10 fields of each section was counted and used to calculate the ratio of apoptotic cells.

2.27. Statistical analysis

Quantitative data are presented as the mean ± standard error of the mean (SEM). Statistical analysis was performed using GraphPad Prism 8.0.2 software (GraphPad Software, La Jolla, CA, USA). The statistical significance of the differences between groups was determined by t tests (for two-group comparisons) or one-way analysis of variance (ANOVA) (for more than two group comparisons), and $P < 0.05$ was considered to indicate statistical significance. The data were obtained from at least three biological replicates, and "n" represents the number of independent samples for each group.

3. Results and discussion

3.1. Disease-derived EVs are enriched with diverse tissue injury-related biomolecules and can be presented to cultured cells

Notably, EV release is a highly conserved process among most cell types, and it has been proposed as a route for removing damaged or unwanted materials from host cells[25]. Consequently, elevated EV secretion or altered EV compositions (such as damage-associated molecular patterns [DAMPs]) have been widely reported in various types of diseases[9,26]. For example, a large prospective clinical study demonstrated that participants with distinct EV-miRNA expression patterns (including miR-2110, miR-24−3p, and miR-193−5p) had an increased risk of declining lung function, and such EV-miRNAs were involved in mediating the lung inflammatory response and airway structural integrity[9]. The EVs released from injured cells can enter the extracellular/pericellular environment and further enter into circulation. Due to the fact that EVs from injured tissue cells carry a large amount of active cargo from donor cells and can be detected in almost all types of body fluids, circulating EVs have been proposed as potential biomarkers for diverse types of tissue injury, such as lung and kidney injury[9].

To explore the changes in EV composition and pathological role in the disease state, public multi-omics data of circulating EVs from different types of tissue injury (such as lung injury and kidney injury) were analyzed[14,15]. Acute respiratory distress syndrome (ARDS) is a severe form of ALI characterized by diffuse alveolar damage and is associated with an increase in alveolar and capillary permeability, thus resulting in interstitial and alveolar edema[14]. Compared with those from healthy controls, the plasma EVs from ARDS patients displayed distinct miRNA expression patterns, as shown by the PCA scatter plot and heatmap (Fig. 2A, left panel). Compared with those in the controls, the plasma EVs in the ARDS patients carried many differentially expressed miRNAs (21 upregulated and 6 downregulated miRNAs), and these altered miRNAs were enriched in pathways related to the hallmarks of ALI pathology, such as inflammation (including TNF signaling and chemokine signaling), immune cell activation (such as Toll-like receptor signaling and T-cell receptor signaling) and fibrosis (such as TGF-β signaling, Fig. 2A, right panel). Similarly, compared with those from healthy controls, serum EVs from diabetic kidney disease (DKD) patients had distinct protein expression patterns (Fig. 2B, left panel). There were also many differentially expressed proteins (394 upregulated and 293 downregulated proteins) in the serum-derived EVs compared to the control EVs, and the upregulated proteins were mainly enriched in the disordered immune response (including the HIF-1 signaling pathway and AGE-RAGE signaling) and disturbed metabolism (such as glycolysis and the pentose phosphate pathway, Fig. 2B, right panel). These pathways are involved in the pathology of DKD[15]. Taken together, these findings suggest that circulating EVs from diseased states are enriched in diverse pathological information and are likely specific to different types of tissue injury.

Afterward, we sought to determine whether circulating EVs from diseased states can identify diverse pathological information about cultured cells. As a proof-of-concept study, it is difficult to include too many disease types in one study; thus, certain critical types of tissue injury in the clinical setting were selected. Both ALI and AKI are critical diseases with high incidence and mortality rates; however, there are no effective treatments for these conditions in the clinical setting[27−29]. Plasma samples from different types of tissue injury, including ALI patients and AKI rats, were collected (Fig. 2C, left panel). ALI is a common disease in critically ill patients with high morbidity and mortality and is characterized by uncontrolled and self-amplified lung inflammation, which can be caused by multiple factors, such as infections, sepsis, and trauma[14]. Severe ALI, such as ARDS, can cause severe systemic inflammation and multiple organ dysfunction, and the mortality of patients with ARDS is 35.3% and 40.0% in intensive care units (ICUs) and hospitals, respectively[28]. AKI is also a serious disease characterized by a rapid decrease in kidney function and can also be caused by trauma, sepsis, surgery, toxic drugs, and other factors[29]. This disorder is estimated to occur in ∼15% of hospital inpatients and up to ∼60% of critically ill patients, and the

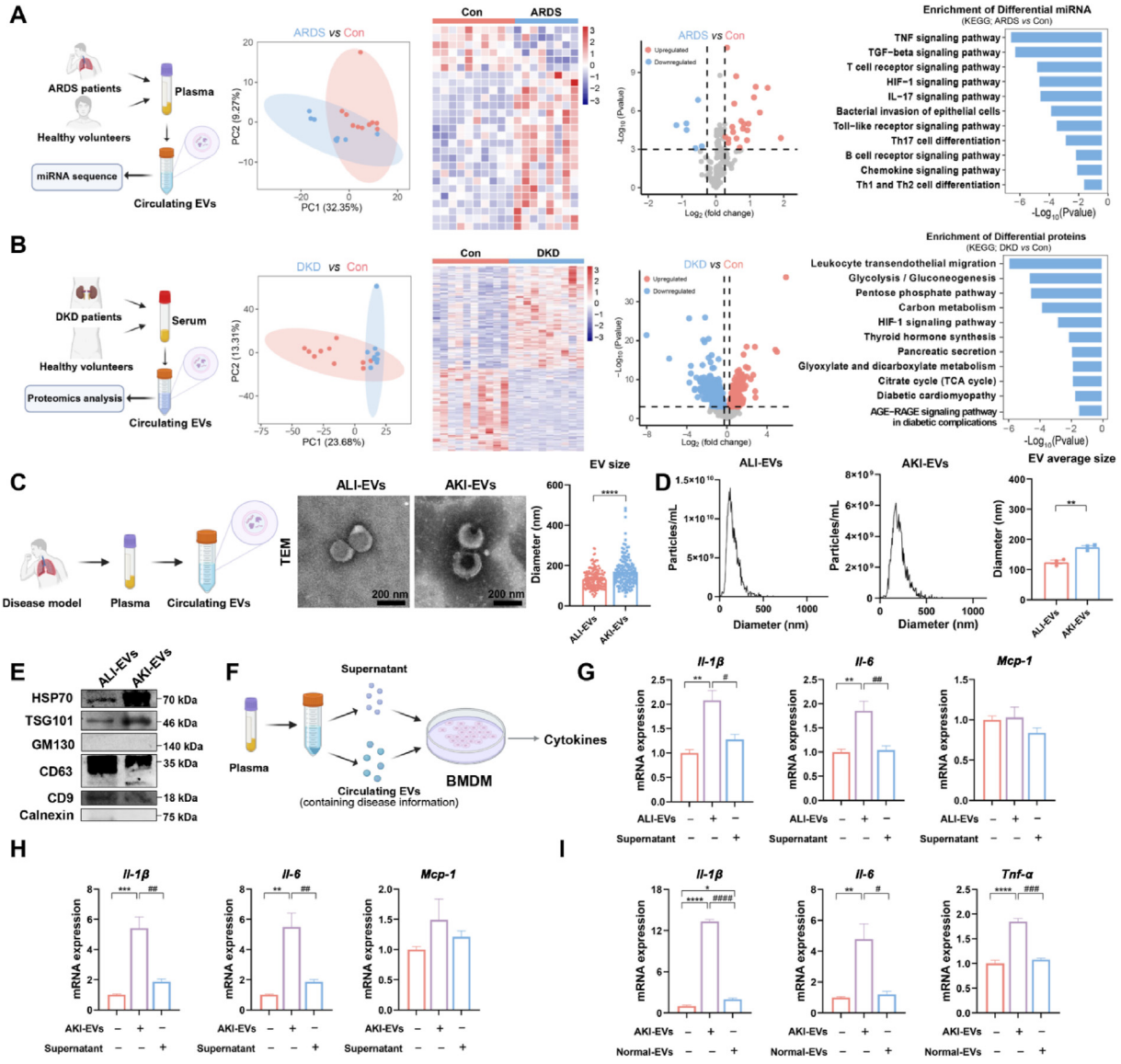

Figure 2 Disease-derived EVs are enriched in diverse tissue injury-related biomolecules and can be presented to cultured cells. (A) The experimental scheme of plasma miRNA sequencing in ARDS patients and healthy volunteers and the representative PCA score plot, differential miRNA heatmap, volcano plot, and KEGG enrichment pathway (n = 8−10). (B) The experimental scheme of serum proteomics in ARDS patients and healthy volunteers and the representative PCA map, differential protein score plot, volcano plot, and KEGG enrichment pathway (n = 10). (C) Experimental schematic of disease-derived EVs isolated from plasma and representative TEM micrographs of ALI-EVs and AKI-EVs (scale bar = 200 nm). The sizes of the ALI-EVs and AKI-EVs were determined by TEM (n = 140 EVs). ****$P < 0.0001$, *vs.* the ALI-EVs group. (D) The size distributions of ALI-EVs and AKI-EVs were measured *via* NTA. The average sizes of the ALI-EVs and AKI-EVs were measured by NTA (n = 3). **$P < 0.01$, *vs.* the ALI-EVs group. (E) Western blot analysis of EV-positive markers (HSP70, TSG101, CD63, and CD9) and a negative control marker (GM130 and Calnexin). (F) Schematic process for evaluating the pathological role of EVs. (G) Cytokine (*Il-1β*, *Il-6*, and *Mcp-1*) levels in macrophages treated with ALI-EVs or EV-free supernatant were measured (n = 3). **$P < 0.01$, *vs.* the Con group; $^{\#}P < 0.05$, $^{\#\#}P < 0.01$, *vs.* the ALI-EV group. (H) Cytokine (*Il-1β* and *Il-6*) and chemokine (*Mcp-1*) levels in BMDMs treated with AKI-EVs or EV-free supernatants were measured (n = 3). **$P < 0.01$, ***$P < 0.001$, *vs.* the Con group; $^{\#\#}P < 0.01$, *vs.* the AKI-EVs group. (I) Cytokine (*Il-1β*, *Il-6*, and *Tnf-α*) levels in BMDMs treated with AKI-EVs or normal EVs were measured (n = 3). *$P < 0.05$, **$P < 0.01$, ****$P < 0.0001$, *vs.* the Con group; $^{\#}P < 0.05$, $^{\#\#\#}P < 0.001$, $^{\#\#\#\#}P < 0.0001$, *vs.* the AKI-EVs group.

mortality rate of severe AKI patients in the ICU can exceed ~60%[27]. For example, cisplatin, a widely used chemotherapeutic drug, can cause severe kidney injury[10], and DNA damage (indicated by 8-OHdG) and related kidney tubular cell death (indicated by TUNEL staining) are hallmarks of cisplatin-induced AKI (Supporting Information Fig. S1).

The purity of EVs isolated from blood samples may be affected by background contamination because blood contains abundant lipoproteins and large numbers of protein particles, such as albumin and globulins[30]. To remove possible contaminants, circulating EVs from plasma samples were isolated by using an optimized differential ultracentrifugation method according to

previous reports[20,31], and the isolated crude EVs were further washed and purified *via* ultracentrifugation. To evaluate the purity of our EV samples, we performed a TEM assay to detect possible contaminants in the crude and purified EVs. High-resolution TEM images revealed the coexistence of many cup-shaped EVs and abundant background contaminants (such as lipoprotein particles) in crude plasma EVs. In contrast, only a few contaminant particles were detected in the purified plasma EVs (Supporting Information Fig. S2), thus suggesting the high purity of the isolated EVs.

The purified EVs that were isolated from the plasma of ALI patients (ALI-EVs) or AKI rats (AKI-EVs) exhibited typical bilayer lipid membrane structures, and their average sizes (as measured by TEM) were 133.8 ± 4.0 and 168.3 ± 6.2 nm, respectively (Fig. 2C). Additionally, the size distribution of disease-derived EVs was analyzed by using NTA, and the average sizes of the ALI-EVs and AKI-EVs were 133.8 ± 4.0 and 168.3 ± 6.2 nm, respectively (Fig. 2D). Interestingly, both the NTA and TEM results showed differences in the size distributions of the ALI-EVs and the AKI-EVs. Although the detailed reason for these results is unclear, the different size distributions of ALI-EVs and AKI-EVs may be due to differences in the species (human *vs.* rat) and/or type of tissue injury (ALI *vs.* AKI). Moreover, these EVs were positive for the endosomal sorting complex required for transport (ESCRT)-associated marker proteins (HSP70 and TSG101) and tetraspanin-related markers (CD63 and CD9) but negative for the Golgi marker GM130 and the endoplasmic reticulum marker Calnexin (Fig. 2E). Together, these results demonstrated that the purified plasma EVs that were used in this study had high purity and less background contamination.

Innate immune cells (such as macrophages) can rapidly switch to a proinflammatory phenotype in response to tissue injury or infection. Thus, macrophages were used as model cells to evaluate the pathological role of disease-derived circulating EVs. EVs and EV-free supernatants were isolated from ALI or AKI plasma, respectively, and subsequently added to bone marrow-derived macrophages (BMDMs) (Fig. 2F) due to the fact that other soluble substances in plasma are also involved in intracellular communication during disease infection. As shown in Supporting Information Fig. S3, the membrane dye MemGlow-labeled plasma EVs were efficiently taken up by macrophages. In line with the findings of previous studies[12,13], plasma EVs or EV-free supernatant could induce cytokine (such as *Il-1β* and *Il-6*) and chemokine (such as *Mcp-1*) expression in macrophages. Compared with those in the EV-free supernatant group, cytokine expression in the disease-EV group was further increased at the same protein concentrations (Fig. 2G and H), thus suggesting an overall increase in innate immune activity triggered by disease-derived EVs. In addition, disease-derived EVs (such as AKI-EVs) had a significantly greater ability to induce cytokine (*Il-1β*, *Il-6*, and *Tnf-α*) expression in macrophages than did plasma EVs from normal controls (Normal-EVs, Fig. 2I). A possible reason for this effect is that disease-derived EVs are enriched in diverse tissue injury-associated molecules, and the lipid bilayer structure of EVs can protect biomolecules (such as RNAs, DNAs, and proteins) from degradation *in vivo*. Taken together, our results suggest that disease-EV preconditioning can efficiently relay diverse tissue injury-related information to cultured cells.

3.2. *Disease-EV preconditioning induces disease-specific gene expression responses in cultured MSCs*

Having shown that disease-derived EVs can transfer pathological information to recipient cells, we aimed to determine whether cultured MSCs have disease-related responses to circulating EVs from different types of tissue injury. To this end, human MSCs (hMSCs) were preconditioned with ALI-EVs or AKI-EVs, after which the changes in the gene expression profiles of the MSCs were analyzed *via* RNA-seq (Fig. 3A). Disease-EVs could be efficiently taken up by MSCs after incubation for 4 h, and there was no significant difference in the uptake rates between ALI-EVs and AKI-EVs (Fig. 3B). A principal component analysis (PCA) scatter plot and heatmap were generated to display marked gene expression pattern alterations between the groups (Fig. 3C, left panel). DEGs affected by disease-derived EVs were identified. There were many DEGs observed in ALI-EV-preconditioned MSCs (ALI-MSCs, 135 upregulated and 152 downregulated mRNAs) and AKI-EV-preconditioned MSCs (AKI-MSCs, 130 upregulated and 183 downregulated mRNAs) compared to those in normally cultured MSCs (NC-MSCs) (Fig. 3D, Fig. S4A and S4B). Among these DEGs, there were more than 90 unique genes between ALI-MSCs (including *NFKBIA*, *JUND*, and *SAMD1*) and AKI-MSCs (including *IFI6*, *IRE2*, and *JUNB*, Fig. 3E).

Further Gene Ontology (GO) pathway enrichment analysis indicated that disease-EV preconditioning induced tissue injury-related gene expression in MSCs due to the fact that these unique genes were strongly enriched in multiple pathways related to ALI (such as IκB kinase/NF-κB signaling and cell-cell adhesion *via* plasma membrane adhesion molecules) and AKI (such as Fas signaling pathway and regulation of membrane depolarization, Fig. 3F, left panel). For example, *NFKBIA* plays an important role in regulating lung inflammation in ALI by enhancing the nuclear translocation of NF-κB and subsequent expression of many proinflammatory genes[32], which are upregulated in ALI-MSCs. Similarly, *IFI6* plays a vital role in regulating renal tubular cell apoptosis in AKI by stabilizing the mitochondrial membrane potential and reducing inflammation[33], which is upregulated in AKI-MSCs. Moreover, there were ∼40 shared DEGs (including *SCD*, *ACAT2*, and *LDLR*) in both the ALI-MSCs and AKI-MSCs, and these genes were enriched in multiple metabolic pathways, such as fatty acid biosynthesis, cholesterol biosynthesis, and phospholipid biosynthesis (Fig. 3F, right panel), thus suggesting that disease-derived EVs may impact the phenotype and biofunctions of MSCs by regulating cell metabolism.

The miRNA profiles of ALI-MSCs and AKI-MSCs were also analyzed by using RNA sequencing because miRNA secretion plays a vital role in regulating the phenotype and therapeutic effects of MSCs[34]. The PCA plot and heatmap showed clear separation and altered miRNA expression in the ALI-MSCs or AKI-MSCs compared to the NC-MSCs (Fig. 3C, right panel, and 3G). The differentially expressed miRNAs (31 upregulated and 9 downregulated miRNAs in ALI-MSCs and 24 upregulated and 10 downregulated miRNAs in AKI-MSCs) in MSCs after disease-EV preconditioning were identified (Supporting Information Fig. S4C and S4D). Compared with those of NC-MSCs, disease-EV-preconditioned MSCs had many unique miRNAs (∼32 miRNAs in ALI-MSCs and 26 miRNAs in AKI-MSCs) and few shared miRNAs (∼8 miRNAs in both types of MSCs, Fig. 3G and H), thus suggesting that different types of disease-derived EVs can induce diverse miRNA expression in MSCs.

Furthermore, the upregulated miRNAs in the ALI-MSCs (including miR-223-3p and miR-486-5p) were enriched in pathways related to the immune response, such as T cell receptor signaling and Th1/Th2 cell differentiation (Fig. 3I), and some of these upregulated miRNAs were strongly associated with lung injury. For example, miR-223 is involved in lung inflammation by

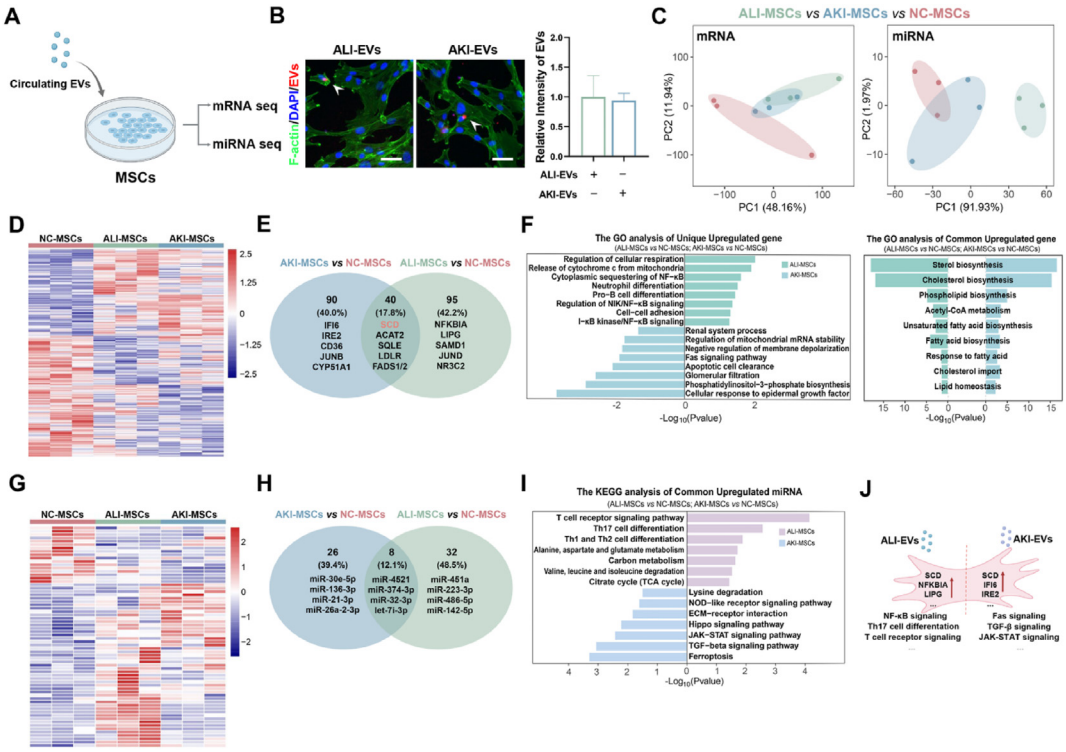

Figure 3 Disease-EV preconditioning induces distinct disease-specific gene expression responses in cultured MSCs. (A) The experimental process of circulating EV-preconditioned MSCs for mRNA and miRNA sequencing ($n = 3$). (B) Representative images of disease-EV uptake stained with phalloidine (green), DAPI (blue), and MemGlow-labeled circulating EVs (red) (scale bar = 200 μm) ($n = 3$). (C) PCA score plot of mRNAs and miRNAs representing discrepancies between different disease-related EV preconditioning regimens. (D) Heatmap of the DEGs between different disease EV preconditioning regimens. (E) Venn diagram representing the number of unique and overlapping genes. (F) GO analysis of the unique (left panel) and common (right panel) genes upregulated in response to preconditioning with different disease-related EVs. (G) Heatmap of the differentially expressed miRNAs between EVs from patients with different diseases. (H) Venn diagram representing the number of unique and overlapping miRNAs. (I) KEGG analysis of the upregulated miRNAs related to precourse treatment with different disease-related EVs. (J) Schematic illustrating the diverse tissue injury-related genes and pathways involved in the preconditioning of MSCs with different disease-related EVs.

regulating monocyte-macrophage differentiation, neutrophil recruitment, and proinflammatory cytokine release[35]. In contrast, the upregulated miRNAs in AKI-MSCs (including miR-21-3p and miR-30e-5p) were enriched in multiple pathways related to cell apoptosis and nephrotoxicity, such as the TGF-β signaling and JAK-STAT pathways (Fig. 3I). Similarly, miR-21a-3p is involved in the pathology of nephropathy by regulating redox metabolic pathways and lipid metabolism[36]. Together, these results suggest that disease-derived EVs can induce distinct and potentially disease-specific gene responses in MSCs (Fig. 3J), and these effects are likely due to the diverse tissue injury-related biomolecules carried by such circulating EVs.

3.3. Disease-EV preconditioning enhances the tissue repair-related performance of MSCs through metabolic rewiring

The survival and therapeutic potency of MSCs are strongly dependent on their cell behaviors, such as cell proliferation, cell migration (such as homing capacity), and paracrine effects (such as growth factor [GF] secretion)[5,6]. Several preconditioning methods (including hypoxia) have been shown to partially increase proliferation rates and the expression of GFs (including hepatocyte growth factor [HGF], fibroblast growth factor 2 [FGF2], and vascular endothelial growth factor [VEGF]) in MSCs[6]. Thus, we evaluated the impact of disease-EV preconditioning on MSC proliferation, migration, and GF production (Fig. 4A). Interestingly, compared with NC-MSCs, MSCs preconditioned with ALI-EVs or AKI-EVs had greater proliferation rates, migration rates, and GF production (*HGF*, *FGF2*, keratinocyte growth factor [*KGF*], and *VEGF*) (Fig. 4B and C), and these GFs are critical for performing tissue repair functions in combination with MSC-based therapies[37]. For example, HGF has been shown to promote epithelial cell proliferation and migration and reduce tubular cell apoptosis in ischemic AKI[38], and VEGF can improve renal tubular cell proliferation and peritubular capillary density while reducing renal tubular epithelial cell apoptosis and renal functional injury in cisplatin-induced AKI[39]. Therefore, these results suggest that disease-EV preconditioning can enhance the overall performance of MSCs; however, the underlying mechanism needs to be further characterized.

The behaviors and repair effects of MSCs are tightly regulated by cell metabolic pathways[40,41]. For example, enhanced lipid metabolism was associated with elevated GF secretion and wound healing ability in MSCs[40]. Thus, the metabolic changes in ALI-MSCs or AKI-MSCs were analyzed by using liquid chromatography-tandem mass spectrometry (LC−MS/MS)-based metabolomics and lipidomics (Fig. 4D). A partial least squares-discriminant analysis (PLS-DA) score plot and heatmap

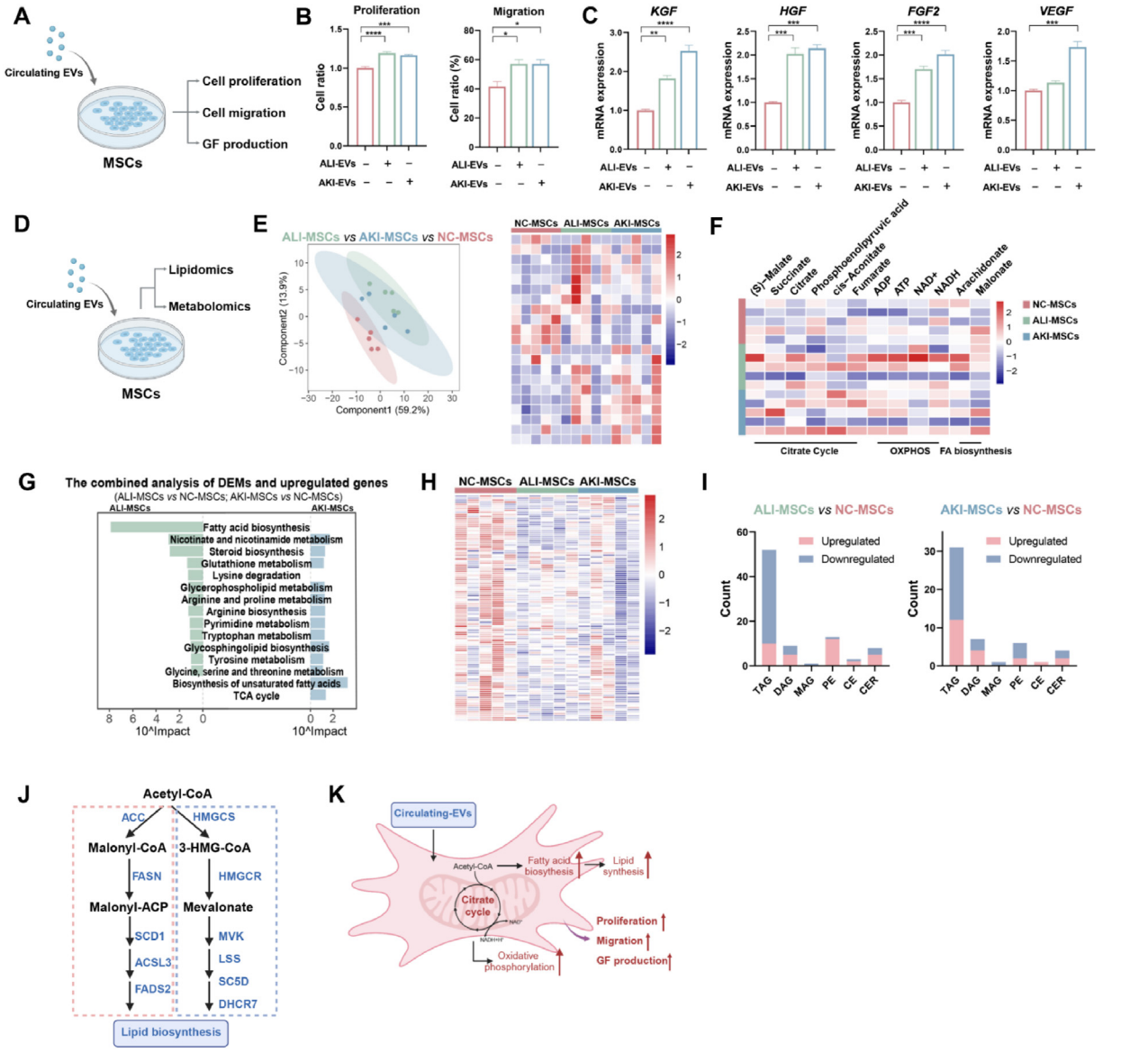

Figure 4 Disease-EV preconditioning enhances the extent of tissue repair mediated by MSCs. (A) Schematic illustrating the evaluation of proliferation, migration, and GF production in MSCs with or without disease-related EVs. (B−C) The proliferation and migration rates and GF (KGF, HGF, FGF2, and VEGF) production of MSCs with or without disease-related EV treatment. $^{*}P < 0.05$, $^{**}P < 0.01$, $^{***}P < 0.001$, $^{****}P < 0.0001$, *vs.* the Con group. (D) The metabolomics and lipidomic data of disease-related EVs preconditioned from MSCs ($n = 5$). (E) The PLS-DA plot and heatmap of metabolites representing discrepancies between different disease-related EV preconditioning methods. (F) Heatmap of the relative abundance of citrate cycle, OXPHOS, and FA biosynthesis metabolites in MSCs treated with or without disease-related EVs. (G) Integrated pathway analysis of upregulated DEGs and differential DEMs. (H) Heatmap of lipids representing discrepancies between preconditioning with different disease-related EVs. (I) The number of lipids that differed between ALI-MSCs or AKI-MSCs and NC-MSCs. (J) The key enzymes involved in lipid biosynthesis. (K) Schematic illustrating the mechanism by which the citrate cycle, OXPHOS, and FA biosynthesis enhance MSC proliferation and migration and GF production in MSCs with diseased EVs.

demonstrated clear separation and distinct metabolite profiles between the groups (Fig. 4E). The metabolites in which expression significantly changed (FC > 1.2, $P < 0.05$) in the ALI-MSCs or AKI-MSCs compared with that in the NC-MSCs were identified (Supporting Information Fig. S5A). We found that, compared with NC-MSCs, disease-EV-preconditioned MSCs had high levels of metabolites involved in the TCA cycle (such as malate, citrate, and aconitate), oxidative phosphorylation (OXPHOS) (such as succinate, ATP, NADH, and NAD^+), and fatty acid (FA) biosynthesis (such as malonate) (Fig. 4F). The $NADPH/NADP^+$ ratio was increased in disease-EV-preconditioned MSCs (Supporting Information Fig. S6).

Afterward, integrated pathway enrichment analysis of the metabolome and transcriptome using significantly altered metabolites and genes was performed, and multiple commonly affected metabolic pathways, such as FA biosynthesis, nicotinate/nicotinamide metabolism, and steroid biosynthesis, were upregulated in both ALI-MSCs and AKI-MSCs (Fig. 4G). Specifically, several such metabolic pathways are involved in cell proliferation and GF production in MSCs[40,41]. For example,

platelet pretreatments were shown to promote GF (including VEGF and HGF) secretion in MSCs by enhancing OXPHOS and FA biosynthesis[40]. NADPH plays a vital role in the biosynthesis of nucleic acids, FAs, cholesterol, and steroid hormones[42]. FAs are important energy substrates and can be oxidized in the mitochondria to fuel the TCA cycle to generate ATP, as well as intermediate metabolites (such as citrate), for other metabolic processes (including FA synthesis)[41]. The process of FA synthesis (FAS) is mediated by multiple enzymatic steps, such as fatty acid synthase (FASN) and acetyl-CoA carboxylase (ACC), which play key roles in regulating membrane lipid formation; thus, they are critical for stem cell division and proliferation[41].

Based on these findings, we examined the impact of disease-EV preconditioning on the lipid profiles, including triglyceride (TAG), diglyceride (DAG), monoglyceride (MAG), phosphatidylethanolamine (PE), sphingomyelin (SM), cholesteryl ester (CE), and ceramide (CER) profiles, of MSCs (Fig. 4D). The PLS-DA plot and heatmap demonstrated clear differences in lipids between the ALI-MSCs or AKI-MSCs group and the NC-MSCs group (Fig. 4H and Fig. S5B). There were more than 110 significantly changed lipids (FC $>$ 1.2, $P < 0.05$) in disease-EV-preconditioned MSCs compared to NC-MSCs (Fig. S5C), and ALI-MSCs or AKI-MSCs had more pronounced changes in multiple lipid types, such as PE, TAGs, and CE, than did NC-MSCs (Fig. 4I). Gene set enrichment analysis (GSEA) based on DEGs from RNA-seq data also demonstrated the upregulation of fatty acid biosynthesis and cholesterol biosynthesis pathways in ALI-MSCs or AKI-MSCs (Fig. 4G and J, Supporting Information Fig. S7). These lipids are essential for cell composition and can regulate diverse cellular processes, such as cell survival and proliferation, energy metabolism, and protein biosynthesis[41,43]. For example, PE and cholesterol are the main structural components of cellular membranes, and TAGs are vital sources of cell energy and can be hydrolyzed into FAs[41,43]. These results collectively suggest that disease-related EVs may enhance the functions of MSCs through metabolic rewiring, such as by enhancing OXPHOS and lipid metabolism (Fig. 4K).

To verify the critical role of metabolic pathways in regulating MSC behaviors, we further disrupted OXPHOS or FA

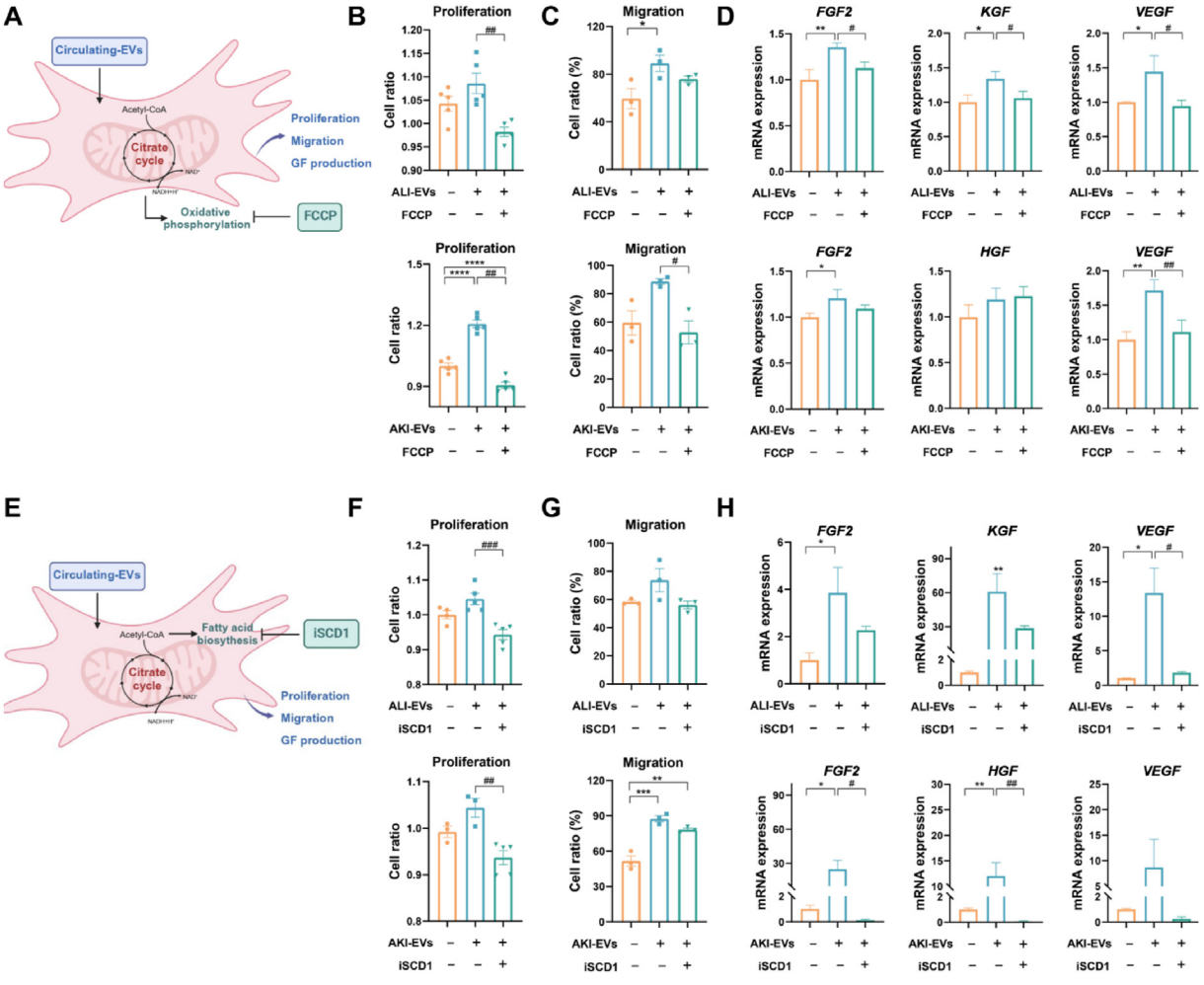

Figure 5 The underlying mechanism of enhanced proliferation, migration, and GF production in cultured MSCs. (A) Schematic illustrating the FCCP treatment experiment ($n = 3-5$). (B–D) The proliferation and migration rates and GF (*FGF2*, *KGF*, *HGF*, and *VEGF*) production in disease-derived EVs preconditioned with MSCs with or without FCCP. $^{*}P < 0.05$, $^{**}P < 0.01$, $^{****}P < 0.0001$, *vs.* the Con group; $^{\#}P < 0.05$, $^{\#\#}P < 0.01$, *vs.* the disease EVs group. (E) Schematic illustrating the iSCD1 treatment experiment ($n = 3-5$). (F–H) Proliferation and migration rates and GF (*FGF2*, *KGF*, *HGF*, and *VEGF*) production in disease-derived EVs preconditioned with MSCs with or without iSCD1. $^{*}P < 0.05$, $^{**}P < 0.01$, *vs.* the Con group; $^{\#}P < 0.05$, $^{\#\#}P < 0.01$, $^{\#\#\#}P < 0.001$, *vs.* the disease EVs group.

biosynthesis and subsequently assessed the changes in cell proliferation, migration, and GF production (Fig. 5A and E). Carbonyl cyanide 4-(trifluoromethoxy) phenylhydrazone (FCCP) can damage mitochondrial OXPHOS and ATP synthesis by disrupting mitochondrial membrane permeability[44]. Stearoyl-CoA desaturase-1 (SCD1) is a key metabolic enzyme of FAS that mediates the biosynthesis of monounsaturated fatty acids from saturated fatty acids and can be effectively blocked by using a specific SCD1 inhibitor (iSCD1, *N*-benzylimidazole carboxamide)[45]. Indeed, the beneficial effects of ALI-EVs and AKI-EVs on promoting MSC proliferation, migration, and GF production were markedly abolished by FCCP or iSCD1 treatment (Fig. 5B−D, F−H). These results collectively suggest that disease-EV preconditioning enhances the proliferation, migration, and GF production of MSCs by boosting OXPHOS and lipid biosynthesis (Fig. 4K). However, it is worth noting that other pathways may also participate in the regulation of these MSC functions because EVs can carry various types of molecules, thus affecting a complicated genetic and metabolic network in recipient cells. Nevertheless, our results indicate that disease-derived EVs can improve MSC functions *in vitro*, and these effects are at least partially due to their impacts on multiple metabolic pathways.

3.4. *Disease-EV preconditioning improves the tissue protective potency of MSCs in vitro*

Having shown that disease-EV preconditioning can induce tissue injury-related gene expression and enhance the function of MSCs, we sought to determine whether disease-EV preconditioning could improve the tissue protective potency of MSCs in diverse cell injury models. For example, ALI is characterized by uncontrolled

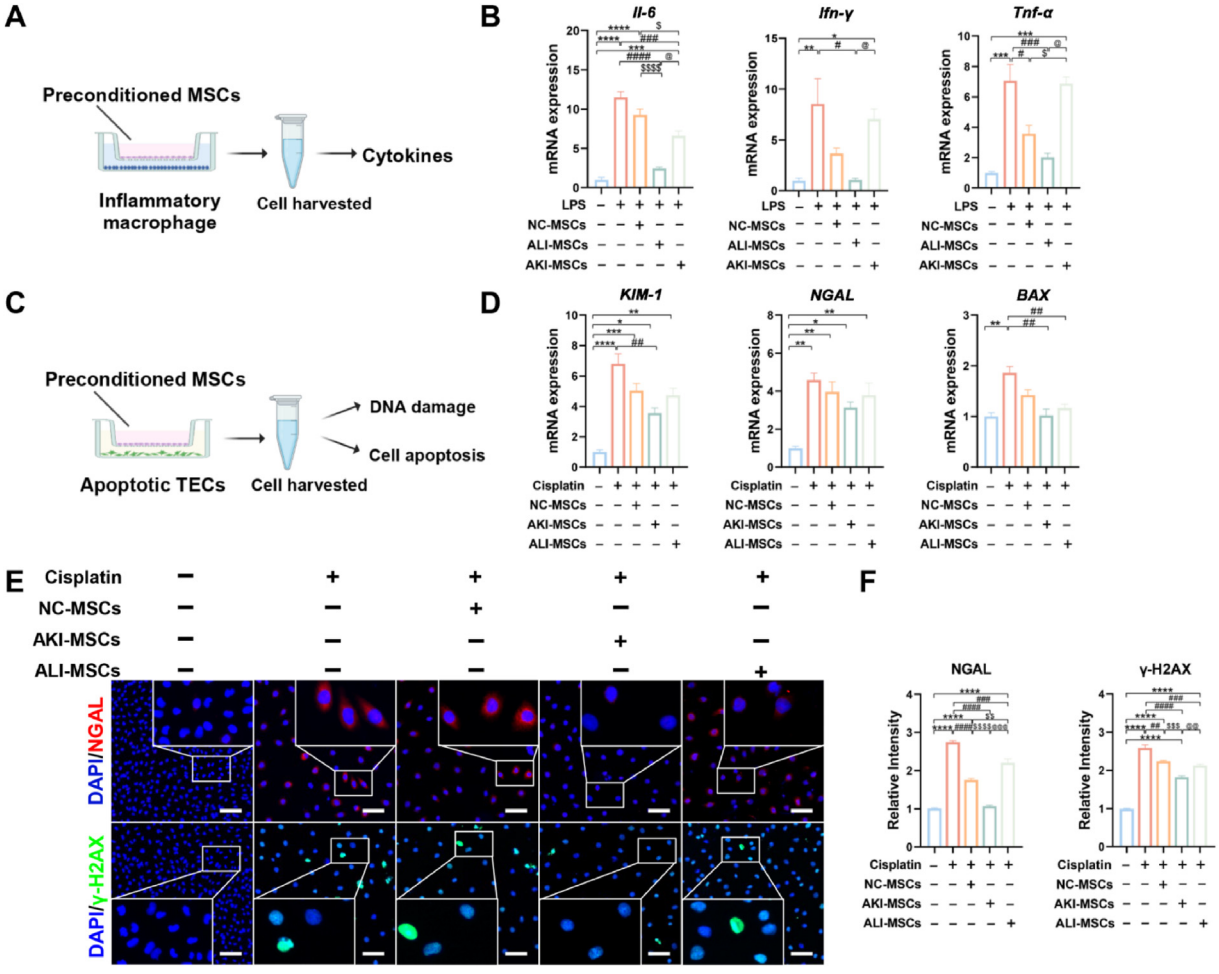

Figure 6 Disease-EV preconditioning improves the tissue-protective potency of MSCs *in vitro*. (A) Experimental scheme for coculturing preconditioned MSCs with LPS-induced inflammatory macrophages ($n = 3$). (B) Measurement of cytokine (*Il-6*, *Ifn-γ*, and *Tnf-α*) mRNA levels in inflammatory macrophages treated with or without NC-MSCs or preconditioned MSCs by qPCR. $^{*}P < 0.05$, $^{**}P < 0.01$, $^{***}P < 0.001$, $^{****}P < 0.0001$, *vs.* the Con group; $^{\#}P < 0.05$, $^{\#\#}P < 0.01$, $^{\#\#\#}P < 0.001$, $^{\#\#\#\#}P < 0.0001$, *vs.* the LPS group; $^{\$}P < 0.05$, $^{\$\$\$\$}P < 0.0001$, *vs.* the NC-MSCs group; $^{@}P < 0.05$, *vs.* the ALI-MSCs group. (C) Experimental scheme of coculturing preconditioned MSCs with cisplatin-induced apoptotic TECs ($n = 3$). (D) Measurement of kidney injury marker (*KIM-1* and *NGAL*) and apoptotic molecule (*BAX*) mRNA levels in apoptotic TECs with or without NC-MSCs or preconditioned MSCs by qPCR. $^{*}P < 0.05$, $^{**}P < 0.01$, $^{***}P < 0.001$, $^{****}P < 0.0001$, *vs.* the Con group; $^{\#\#}P < 0.01$, *vs.* the Cisplatin group. (E) Representative images of renal tubular epithelial cell NGAL and γ-H2AX IF staining (scale bar = 100 μm). (F) Quantitative analysis of NGAL and γ-H2AX protein expression. $^{****}P < 0.0001$, *vs.* the Con group; $^{\#\#}P < 0.01$, $^{\#\#\#}P < 0.001$, $^{\#\#\#\#}P < 0.0001$, *vs.* the Cisplatin group; $^{\$\$}P < 0.01$, $^{\$\$\$}P < 0.001$, $^{\$\$\$\$}P < 0.0001$, *vs.* the NC-MSCs group; $^{@@}P < 0.01$, $^{@@@}P < 0.001$, *vs.* the AKI-MSCs group.

lung inflammation, and abnormally activated infiltrating innate immune cells (such as macrophages and neutrophils) can secrete excessive proinflammatory factors, such as *Il-1β*, *Il-6*, and *Tnf-α*, which correspondingly exacerbates lung inflammation and tissue injury, whereas MSC therapies have been reported to suppress cytokine release in macrophages in ALI models[4,46]. LPS, which is the major component of the outer membrane of gram-negative bacteria, can cause an inflammatory response in lung macrophages[4]. Thus, LPS-induced proinflammatory macrophages were used as a model to assess the therapeutic effects of disease-EV-preconditioned MSCs by using a Transwell system-based cell coculture assay (Fig. 6A). In line with the findings of previous reports, LPS-primed macrophages exhibited elevated cytokine (*Il-6*, *Ifn-γ*, and *Tnf-α*) gene expression compared with that in the control group, whereas this cytokine could be suppressed by coculture with NC-MSCs, ALI-MSCs or AKI-MSCs (Fig. 6B). Importantly, compared with those in the NC-MSCs group, the expression of certain cytokines (*Il-6*) in macrophages cocultured with ALI-MSCs was lower (Fig. 6B), thus suggesting that ALI-MSCs may have greater anti-inflammatory effects than NC-MSCs or AKI-MSCs.

Unlike ALI, toxin (such as cisplatin)-induced AKI is characterized by DNA damage and renal tubular epithelial cell (TEC) death due to the fact that TECs are sensitive to toxins[47]. In the present study, TECs with cisplatin-induced damage were used as a model to evaluate the renoprotective effect of MSCs *in vitro* (Fig. 6C). Cisplatin stimulation damaged TECs and increased the levels of DNA damage markers (γ-H2AX), AKI markers (*KIM-1* and *NGAL*), and proapoptotic signals (*BAX*) in human TECs (HK-2 cells) (Fig. 6D−F). In contrast, MSC coculture markedly decreased the expression of NGAL, *BAX*, and γ-H2AX in injured TECs, and the levels of NGAL and γ-H2AX were lower in TECs from the AKI-MSC group than in those from the NC-MSCs or ALI-MSCs group (Fig. 6D−F). In addition, MSCs were preconditioned with plasma EVs from normal healthy rats (Nor-MSCs) or AKI rats (AKI-MSCs), and their protective effect on TEC injury was also evaluated *in vitro*. The results showed that TECs from the Nor-MSCs group had greater expression of *KIM-1* than those from the AKI-MSCs group (Supporting Information Fig. S8A and B). These results indicate that disease-EV preconditioning is a potential method for specifically enhancing the therapeutic efficacy of MSCs, and this effect is likely a joint effect of the tissue injury-related gene response and metabolic rewiring of MSCs.

3.5. In vivo distribution and immunogenic assay of disease-EV-preconditioned MSCs

Before *in vivo* MSC therapy, we determined whether the *in vivo* distribution pattern of MSCs was affected by EV preconditioning by using different types of tissue injury or tissue injury models. MSCs from different groups were labeled with DiD (a near-infrared dye), and these cells were subsequently injected into mice *via* systemic (intraperitoneal i.p.] or i.v.) injection (Fig. 7A and D). In LPS-induced ALI mice, intravenously (i,v,)-injected NC-MSCs or ALI-MSCs primarily accumulated in the lung and had lower signals in the liver, spleen, and kidneys at 24 h after i.v. injection; however, there was no significant difference in the MSC signals in the lung tissues between the two groups (Fig. 7B and C). In cisplatin-induced AKI mice, IP-injected NC-MSCs or AKI-MSCs primarily accumulated in the liver, and few signals accumulated in the kidneys; moreover, there was no significant difference in the MSC signals in the lung tissues between the two groups (Fig. 7E and F). These results suggest that disease-EV preconditioning has a minimal impact on MSC distribution *in vivo*. A possible explanation is that MSCs are relatively large (∼15−30 μm in diameter) and can be largely trapped in the capillary system of lung tissues after IV injection[48], whereas IP-injected MSCs may avoid primary vascular trapping in lung tissues and thereby have improved retention in other organs (such as the kidneys)[49]. Thus, to improve the tissue repair role of MSC therapies, in addition to cell modification, it is vital to select a proper cell administration route according to the tissue injury type.

In addition, the impact of disease EV-preconditioned MSCs on innate immune cells (macrophages) response was assessed by using an *in vitro* coculture system. Many previous studies have reported the ability of MSC therapy to facilitate the repair and regeneration of damaged tissue through their immunomodulatory actions, and no obvious adverse events resulting from MSC transplantation were observed in clinical trials[50]. It has been reported that MSCs can avoid adverse host immune responses

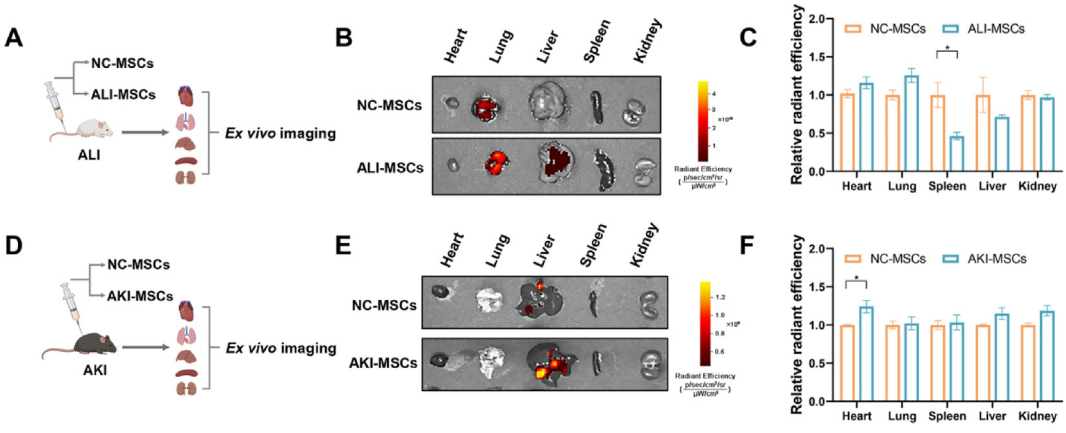

Figure 7 *In vivo* distribution of disease-EV-preconditioned MSCs in micec (A) Schematic illustrating the biodistribution of MSCs in ALI mice with or without ALI-EV preconditioning ($n = 3$). (B) Representative IVIS images of organs harvested from mice at 24 h after intravenous injection of DiD-labeled MSCs. (C) Quantification of the fluorescence intensity in organs from ALI mice. $^*P < 0.05$, *vs.* the NC-MSCs group. (D) Schematic illustrating the biodistribution of AKI-EV-preconditioned MSCs in AKI mice ($n = 3$). (E) Representative IVIS images of organs harvested from mice at 48 h after intravenous injection of DiD-labeled MSCs. (F) Quantification of the fluorescence intensity in organs from AKI mice. $^*P < 0.05$, *vs.* the NC-MSCs group.

because they do not express human leukocyte antigen (HLA) class II or many costimulatory molecules[51]. Similarly, there was no significant difference in the expression of cytokines (*Il-1β* and *Tnf-α*) between the NC-MSCs group and the ALI-MSCs or AKI-MSCs group (Supporting Information Fig. S9), which indicates that disease EV-preconditioned MSCs do not induce adverse immune responses and have good biocompatibility.

3.6. *Disease-EV preconditioning improves the tissue repair potency of MSCs in diverse forms of tissue injury in vivo*

Having demonstrated the enhanced protective capacity of disease-EV-preconditioned MSCs *in vitro*, we next evaluated the tissue repair effects of these MSCs in different types of tissue injury models (mouse ALI and mouse AKI, Fig. 8A and E) due to the

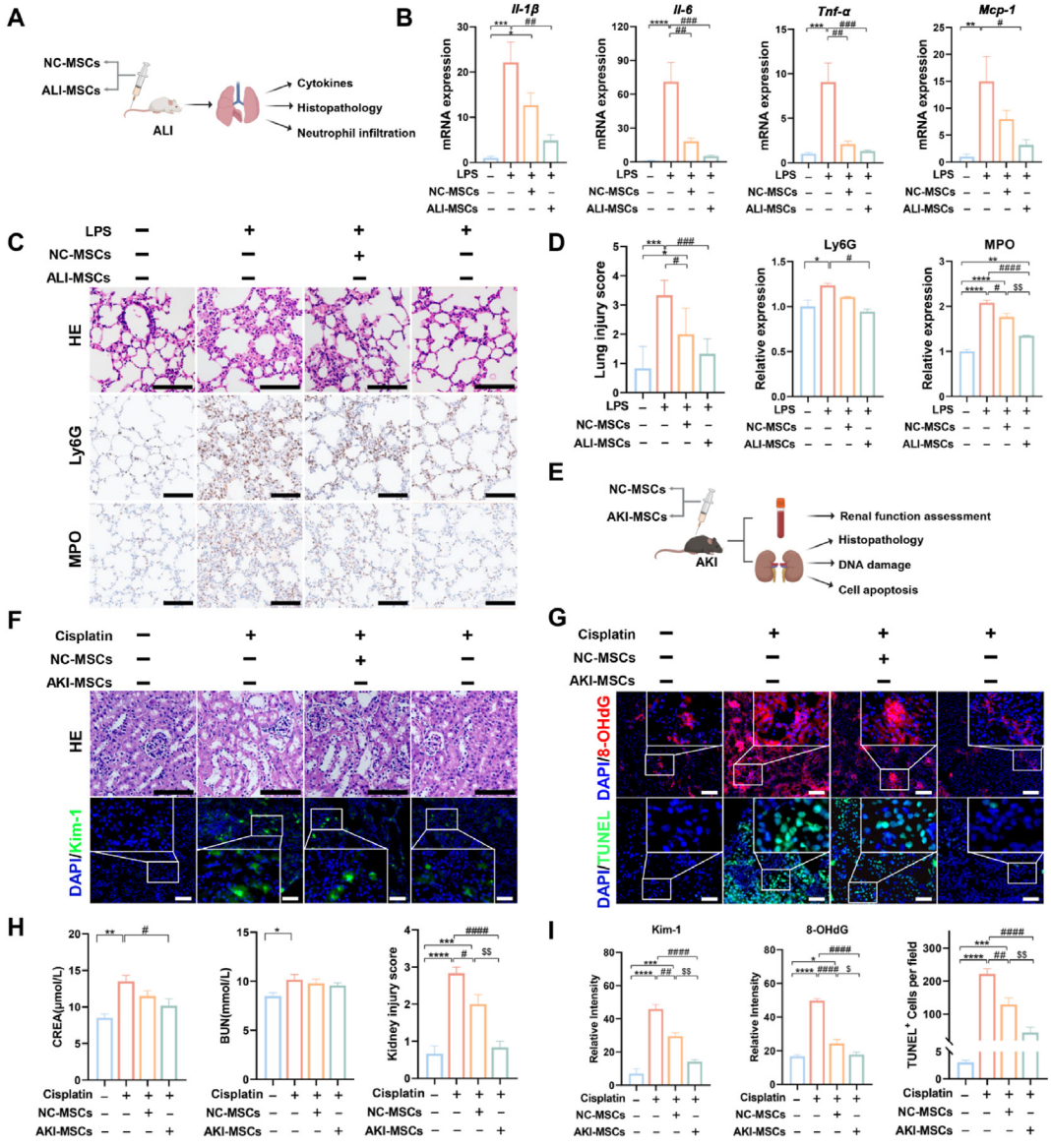

Figure 8 Disease-EV preconditioning improves the tissue repair potency of MSCs in diverse forms of tissue injury *in vivo*. (A) Experimental scheme of ALI induction and treatment ($n = 3–6$). (B) Measurement of cytokine (*Il-1β*, *Il-6*, and *Tnf-α*) and chemokine (*Mcp-1*) mRNA levels in the lungs of ALI mice treated with or without NC-MSCs or ALI-MSCs by qPCR. $^{*}P < 0.05$, $^{**}P < 0.01$, $^{***}P < 0.001$, $^{****}P < 0.0001$, *vs.* the Con group; $^{\#}P < 0.05$, $^{\#\#}P < 0.01$, $^{\#\#\#}P < 0.001$, *vs.* the LPS group. (C) Representative images of H&E-stained lungs (scale bar = 100 μm) and Ly6G and MPO IHC staining (scale bar = 100 μm). (D) Quantitative analysis of the lung injury score and Ly6G and MPO protein expression. $^{*}P < 0.05$, $^{**}P < 0.01$, $^{***}P < 0.001$, $^{****}P < 0.0001$, *vs.* the Con group; $^{\#}P < 0.05$, $^{\#\#\#}P < 0.001$, $^{\#\#\#\#}P < 0.0001$, *vs.* the LPS group. $^{\$\$}P < 0.01$, *vs.* the NC-MSCs group. (E) Experimental scheme of AKI induction and treatment ($n = 3–6$). (F–G) Representative images of renal H&E staining (scale bar = 100 μm), Kim-1 and 8-OHdG IF staining (scale bar = 100 μm), and TUNEL staining (scale bar = 50 μm). (H) The kidney injury score and serum BUN and CREA levels 48 h after AKI. $^{*}P < 0.05$, $^{**}P < 0.01$, $^{***}P < 0.001$, $^{****}P < 0.0001$, *vs.* the Con group; $^{\#}P < 0.05$, $^{\#\#\#\#}P < 0.0001$, *vs.* the Cisplatin group. $^{\$\$}P < 0.01$, *vs.* the NC-MSCs group. (I) Quantitative analysis of Kim-1 and 8-OHdG protein expression and TUNEL^{+} cells. $^{*}P < 0.05$, $^{***}P < 0.001$, $^{****}P < 0.0001$, *vs.* the Con group; $^{\#\#}P < 0.01$, $^{\#\#\#\#}P < 0.0001$, *vs.* the Cisplatin group. $^{\$}P < 0.05$, $^{\$\$}P < 0.01$, *vs.* the NC-MSCs group.

fact that MSC therapies were shown to suppress lung inflammation in LPS-induced ALI models and reduce oxidative stress and TEC death in cisplatin-induced AKI models[3,4]. We found that LPS-induced ALI mice had severe lung lesions (thickened alveolar septa, alveolar hemorrhage, and edema), increased cytokine (MPO, *Il-1β*, *Il-6*, *Tnf-α*, and *Mcp-1*) expression and $Ly6G^+$ neutrophil infiltration in lung tissues; these lung injuries could be partially attenuated after treatment with NC-MSCs or ALI-MSCs *via* i.v. injection (Fig. 8B−D). Moreover, the lung tissues of the ALI-MSCs exhibited lower lung injury scores, $Ly6G^+$ neutrophil numbers, and cytokine levels (such as MPO) than did those of the NC-MSCs (Fig. 8B−D), thus suggesting that, compared with NC-MSCs, ALI-MSCs have greater anti-inflammatory potency and a greater lung protective effect.

In the case of AKI, compared with normal mice, cisplatin-induced AKI mice exhibited histological lesions (tubular swelling, necrosis, and cast formation in the tubular lumen) and increased serum CREA/BUN, Kim-1^+ injured renal tubules and 8-OHdG (which is a marker of DNA damage) expression in kidney tissues (Fig. 8F−I). The degree of kidney injury in AKI mice was alleviated after NC-MSCs or AKI-MSCs treatment, as indicated by the reduced serum CREA/BUN and kidney injury score compared to those in mice with AKI alone (Fig. 8H). Importantly, kidney tissues from the AKI-MSCs group exhibited lower levels of Kim-1^+, 8-OHdG, and $TUNEL^+$ apoptotic cells than did those from the NC-MSCs group (Fig. 8F−I), thus suggesting that AKI-MSCs have greater antiapoptotic and renoprotective effects than do NC-MSCs. Taken together, our results suggest that disease-EV preconditioning is a promising approach for precisely enhancing the tissue repair potential of MSC-based therapies both *in vitro* and *in vivo*.

Furthermore, disease-derived EVs may serve as a type of 'off-the-shelf' product for MSC preconditioning compared to some conventional preconditioning methods, such as biomolecule (including cytokines and whole biofluid) or mechanical/stress stimulation (such as 3D culture and hypoxia) methods, due to multiple advantages, such as stability, long-term storage, and ease of shipment and use. For example, the unique lipid bilayer structure of EVs can provide protection against biomolecules within EVs, which are more stable than free biomolecules (such as cytokines and RNAs) in solution[52]. Additionally, multiple storage techniques that can preserve long-term EV bioactivities, such as freezing, lyophilization, and spray drying, have been developed[8,52]. For example, EVs in a buffered saline solution are stable for up to 2 years at −80 °C without significant changes in their properties, and the bioactivities of lyophilized EVs are similar to those of frozen EVs, even when stored at room temperature for 4 weeks[8]. Moreover, circulating EVs can be readily noninvasively and reproducibly isolated from the biofluid of patients because EV-based liquid biopsy methods have been widely studied and may be useful as biomarkers for obtaining multiple diagnostic agents.

Although our results indicate that disease-EV preconditioning is a potent method to precisely enhance the tissue repair role of MSCs through metabolic reprogramming, many questions have not been answered. For example, we cannot exclude the possibility that other pathways, as well as the detailed effector molecules within disease-derived EVs, may contribute to these effects due to the fact that circulating EVs can carry various types of molecules and thereby affect complex signaling networks in MSCs. Additionally, the *in vivo* efficacy of transplanted MSCs can be affected by multiple factors, and the detailed fate of preconditioned MSCs needs further clarification. However, the pathogenesis of tissue injury is complicated; for instance, multiple types of cell injury and various intracellular processes, such as oxidative stress, mitochondrial damage, cell death, and the inflammatory response, are involved in the pathology of AKI[29]. In the present study, we evaluated the therapeutic efficacy of MSC treatment in reducing DNA damage and tubular apoptosis but did not assess the impact of MSCs on other pathological factors in injured renal tubular cells and other types of kidney tissue cells, which needs to be further explored.

Indeed, the translation of disease-EV-preconditioned MSCs into clinical applications still faces many challenges. To date, despite the existence of strong preclinical data, relatively few clinical trials using preconditioning MSCs have been conducted (fewer than ten studies), whereas more (hundreds of studies) clinical trials using native MSCs have been registered for treating various diseases[53]. In the present study, we only tested the effects of disease-derived EVs from limited types of tissue injury (ALI and AKI) on MSC function, and the role of preconditioned MSCs in tissue repair was evaluated in mouse models. In addition, the long-term *in vivo* immune response after MSC transplantation remains elusive. To further verify the clinical translational potential of disease-EV-preconditioned methods, more efficacy and biosafety assays using more types of diseased EV sources and larger animal models of tissue injury are needed in future studies. Nevertheless, this study highlights the idea that disease-EV preconditioning *via* MSC-based precision medicine is a potent strategy for treating diverse forms of tissue injury and is worthy of further exploration in future studies.

Conclusions

In summary, our results indicate that disease-EV preconditioning is a potential strategy for enhancing the tissue-specific repair effects of MSC therapy. Disease-EVs can transfer various tissue injury-related molecules into in vitro cultured MSCs and further boost their biological functions by inducing metabolic rewiring. Importantly, MSCs preconditioned with disease-EVs exert improved protective roles in different types of tissue injury models. This study highlights that disease-EV preconditioning can enhance the therapeutic potency of MSCs and it is a promising strategy for precision stem cell therapy.

Acknowledgments

This study was partly supported by the National Natural Science Foundation of China (32071453, 32271438, and 31871001 to Jingping Liu) and the 1.3.5 Project for Disciplines of Excellence (ZYYC23001 to Jingping Liu, China), West China Hospital of Sichuan University. The authors thank Na Jiang at the Advanced Mass Spectrometry Center, Research Core Facility, West China Hospital of Sichuan University for providing technical assistance with metabolomic and lipidomic analysis. The authors thank YuZhen SuoLang from the Department of Emergency Medicine, West China Hospital of Sichuan University, for collecting patients' blood. All the experimental schemes were created with BioRender.com.

Authors contribution

Ke Lv: Writing − review & editing, Writing − original draft, Visualization, Validation, Software, Resources, Methodology,

Investigation, Formal analysis, Data curation, Conceptualization. Tian Wu: Visualization, Methodology. Shuyun Liu: Methodology. Peng Lou: Methodology. Pingya Zhou: Methodology. Yizhuo Wang: Methodology. Xiyue Zhou: Methodology. Shu Zhang: Resources. Dan Du: Methodology. Yanrong Lu: Supervision. Meihua Wan: Writing − review & editing, Resources, Methodology. Jingping Liu: Writing − review & editing, Project administration, Methodology, Investigation, Funding acquisition, Conceptualization.

Conflict of interest

The authors declare that they have no competing interests in this work.

Appendix A. Supporting information

Supporting information to this article can be found online at https://doi.org/10.1016/j.apsb.2024.06.027.

References

1. Margiana R, Markov A, Zekiy AO, Hamza MU, Al-Dabbagh KA, Al-Zubaidi SH, et al. Clinical application of mesenchymal stem cell in regenerative medicine: a narrative review. *Stem Cell Res Ther* 2022;**13**:366.
2. Zhou J, Shi YF. Mesenchymal stem/stromal cells (MSCs): origin, immune regulation, and clinical applications. *Cell Mol Immunol* 2023;**20**:555−7.
3. Ullah M, Liu DD, Rai S, Dadhania A, Jonnakuti S, Concepcion W, et al. Reversing acute kidney injury using pulsed focused ultrasound and MSC therapy: a role for HSP-mediated PI3K/AKT signaling. *Mol Ther Methods Clin Dev* 2020;**17**:683−94.
4. Xiao K, He WX, Guan W, Hou F, Yan P, Xu JQ, et al. Mesenchymal stem cells reverse EMT process through blocking the activation of NF-κB and Hedgehog pathways in LPS-induced acute lung injury. *Cell Death Dis* 2020;**11**:863.
5. Hu CX, Li LJ. Preconditioning influences mesenchymal stem cell properties *in vitro* and *in vivo*. *J Cell Mol Med* 2018;**22**:1428−42.
6. Yin JQ, Zhu J, Ankrum JA. Manufacturing of primed mesenchymal stromal cells for therapy. *Nat Biomed Eng* 2019;**3**:90−104.
7. Fan XL, Zhang Y, Li X, Fu QL. Mechanisms underlying the protective effects of mesenchymal stem cell-based therapy. *Cell Mol Life Sci* 2020;**77**:2771−94.
8. Lv K, Wang YZ, Lou P, Liu SY, Zhou PY, Yang L, et al. Extracellular vesicles as advanced therapeutics for the resolution of organ fibrosis: current progress and future perspectives. *Front Immunol* 2022;**13**:1042983.
9. Eckhardt CM, Gambazza S, Bloomquist TR, De Hoff P, Vuppala A, Vokonas PS, et al. Extracellular vesicle-encapsulated microRNAs as novel biomarkers of lung health. *Am J Respir Crit Care Med* 2023;**207**:50−9.
10. Lou P, Liu SY, Wang YZ, Lv K, Zhou XY, Li L, et al. Neonatal-tissue-derived extracellular vesicle therapy (NEXT): a potent strategy for precision regenerative medicine. *Adv Mater* 2023;**35**:e2300602.
11. Wang YZ, Lou P, Xie YJ, Liu SY, Li L, Wang CS, et al. Nutrient availability regulates the secretion and function of immune cell-derived extracellular vesicles through metabolic rewiring. *Sci Adv* 2024;**10**:eadj1290.
12. Jiang K, Yang J, Guo S, Zhao G, Wu H, Deng G. Peripheral circulating exosome-mediated delivery of miR-155 as a novel mechanism for acute lung inflammation. *Mol Ther* 2019;**27**:1758−71.
13. Carrascal M, Areny-Balagueró A, de-Madaria E, Cárdenas-Jaén K, García-Rayado G, Rivera R, et al. Inflammatory capacity of exosomes released in the early stages of acute pancreatitis predicts the severity of the disease. *J Pathol* 2022;**256**:83−92.
14. Parzibut G, Henket M, Moermans C, Struman I, Louis E, Malaise M, et al. A blood exosomal miRNA signature in acute respiratory distress syndrome. *Front Mol Biosci* 2021;**8**:640042.
15. Nunez Lopez YO, Iliuk A, Petrilli AM, Glass C, Casu A, Pratley RE. Proteomics and phosphoproteomics of circulating extracellular vesicles provide new insights into diabetes pathobiology. *Int J Mol Sci* 2022;**23**:5779.
16. Ru Y, Kechris KJ, Tabakoff B, Hoffman P, Radcliffe RA, Bowler R, et al. The multiMiR R package and database: integration of microRNA-target interactions along with their disease and drug associations. *Nucleic Acids Res* 2014;**42**:e133.
17. Wu TZ, Hu EQ, Xu SB, Chen MJ, Guo PF, Dai ZH, et al. clusterProfiler 4.0: a universal enrichment tool for interpreting omics data. *Innovation (Camb)* 2021;**2**:100141.
18. World Medical Association Declaration of Helsinki: Ethical principles for medical research involving human subjects. *JAMA* 2013;**310**:2191−4.
19. Lin QH, Shen J, Shen LH, Zhang ZW, Fu FM. Increased plasma levels of heparin-binding protein in patients with acute respiratory distress syndrome. *Crit Care* 2013;**17**:R155.
20. Yang J, Gao X, Xing XT, Huang HS, Tang Q, Ma SX, et al. An isolation system to collect high quality and purity extracellular vesicles from serum. *Int J Nanomedicine* 2021;**16**:6681−92.
21. Théry C, Witwer KW, Aikawa E, Alcaraz MJ, Anderson JD, Andriantsitohaina R, et al. Minimal information for studies of extracellular vesicles 2018 (MISEV2018): a position statement of the International Society for Extracellular Vesicles and update of the MISEV2014 guidelines. *J Extracell Vesicles* 2018;**7**:1535750.
22. Lv K, Lou P, Liu SY, Wang YZ, Yang JL, Zhou PY, et al. Injectable Multifunctional composite hydrogel as a combination therapy for preventing postsurgical adhesion. *Small* 2024;**20**:e2303425.
23. Du D, Gu HW, Djukovic D, Bettcher L, Gong M, Zheng W, et al. Multiplatform metabolomics investigation of antiadipogenic effects on 3T3-L1 adipocytes by a potent diarylheptanoid. *J Proteome Res* 2018;**17**:2092−101.
24. Tripura C, Gunda S, Vishwakarma SK, Thatipalli AR, Jose J, Jerald MK, et al. Long-term and non-invasive *in vivo* tracking of DiD dye-labeled human hepatic progenitors in chronic liver disease models. *World J Hepatol* 2022;**14**:1884−98.
25. Zhou XY, Liu SY, Lu YR, Wan MH, Cheng JQ, Liu JP. MitoEVs: a new player in multiple disease pathology and treatment. *J Extracell Vesicles* 2023;**12**:e12320.
26. Hallal S, Tűzesi Á, Grau GE, Buckland ME, Alexander KL. Understanding the extracellular vesicle surface for clinical molecular biology. *J Extracell Vesicles* 2022;**11**:e12260.
27. Pickkers P, Darmon M, Hoste E, Joannidis M, Legrand M, Ostermann M, et al. Acute kidney injury in the critically ill: an updated review on pathophysiology and management. *Intensive Care Med* 2021;**47**:835−50.
28. Pham T, Rubenfeld GD. Fifty years of research in ARDS. The epidemiology of acute respiratory distress syndrome. A 50th birthday review. *Am J Respir Crit Care Med* 2017;**195**:860−70.
29. Hoste EAJ, Kellum JA, Selby NM, Zarbock A, Palevsky PM, Bagshaw SM, et al. Global epidemiology and outcomes of acute kidney injury. *Nat Rev Nephrol* 2018;**14**:607−25.
30. Simonsen JB. What are we looking at? Extracellular Vesicles, lipoproteins, or both?. *Circ Res* 2017;**121**:920−2.
31. André-Grégoire G, Roux Q, Gavard J. Isolating plasma extracellular vesicles from mouse blood using size-exclusion chromatography, density gradient, and ultracentrifugation. *STAR Protoc* 2023;**4**:102740.
32. Wang XS, Zhou LY, Ye SS, Liu SD, Chen L, Cheng ZZ, et al. rFGF4 alleviates lipopolysaccharide-induced acute lung injury by inhibiting

the TLR4/NF-κB signaling pathway. *Int Immunopharmacol* 2023;**117**:109923.
33. Chen J, Liu YW, Xia S, Ye XJ, Chen L. Annexin A2 (ANXA2) regulates the transcription and alternative splicing of inflammatory genes in renal tubular epithelial cells. *BMC Genomics* 2022;**23**:544.
34. Xu HK, Chen LJ, Zhou SN, Li YF, Xiang C. Multifunctional role of microRNAs in mesenchymal stem cell-derived exosomes in treatment of diseases. *World J Stem Cells* 2020;**12**:1276−94.
35. Roffel MP, Bracke KR, Heijink IH, Maes T. miR-223: a key regulator in the innate immune response in asthma and COPD. *Front Med (Lausanne)* 2020;**7**:196.
36. Chau BN, Xin C, Hartner J, Ren S, Castano AP, Linn G, et al. MicroRNA-21 promotes fibrosis of the kidney by silencing metabolic pathways. *Sci Transl Med* 2012;**4**:121ra18.
37. Han Y, Yang J, Fang J, Zhou Y, Candi E, Wang J, et al. The secretion profile of mesenchymal stem cells and potential applications in treating human diseases. *Signal Transduct Target Ther* 2022;**7**:92.
38. Liu SY, Zhao M, Zhou YJ, Li L, Wang CS, Yuan YJ, et al. A self-assembling peptide hydrogel-based drug co-delivery platform to improve tissue repair after ischemia-reperfusion injury. *Acta Biomater* 2020;**103**:102−14.
39. Yuan L, Wu MJ, Sun HY, Xiong J, Zhang Y, Liu CY, et al. VEGF-modified human embryonic mesenchymal stem cell implantation enhances protection against cisplatin-induced acute kidney injury. *Am J Physiol Renal Physiol* 2011;**300**:F207−18.
40. Levoux J, Prola A, Lafuste P, Gervais M, Chevallier N, Koumaiha Z, et al. Platelets facilitate the wound-healing capability of mesenchymal stem cells by mitochondrial transfer and metabolic reprogramming. *Cell Metab* 2021;**33**:283−299.e9.
41. Clémot M, Sênos Demarco R, Jones DL. Lipid mediated regulation of adult stem cell behavior. *Front Cell Dev Biol* 2020;**8**:115.
42. Xiao W, Wang RS, Handy DE, Loscalzo J. NAD(H) and NADP(H) redox couples and cellular energy metabolism. *Antioxid Redox Signal* 2018;**28**:251−72.
43. Calzada E, Onguka O, Claypool SM. Phosphatidylethanolamine metabolism in health and disease. *Int Rev Cell Mol Biol* 2016;**321**:29−88.
44. Koncha RR, Ramachandran G, Sepuri NBV, Ramaiah KVA. CCCP-induced mitochondrial dysfunction—characterization and analysis of integrated stress response to cellular signaling and homeostasis. *FEBS J* 2021;**288**:5737−54.
45. Atkinson KA, Beretta EE, Brown JA, Castrodad M, Chen Y, Cosgrove JM, et al. *N*-**B**enzylimidazole carboxamides as potent, orally active stearoylCoA desaturase-1 inhibitors. *Bioorg Med Chem Lett* 2011;**21**:1621−5.
46. Xia LJ, Zhang CL, Lv NY, Liang ZH, Ma TH, Cheng HB, et al. AdMSC-derived exosomes alleviate acute lung injury *via* transferring mitochondrial component to improve homeostasis of alveolar macrophages. *Theranostics* 2022;**12**:2928−47.
47. Tang CY, Livingston MJ, Safirstein R, Dong Z. Cisplatin nephrotoxicity: new insights and therapeutic implications. *Nat Rev Nephrol* 2023;**19**:53−72.
48. Zhuang WZ, Lin YH, Su LJ, Wu MS, Jeng HY, Chang HC, et al. Mesenchymal stem/stromal cell-based therapy: mechanism, systemic safety and biodistribution for precision clinical applications. *J Biomed Sci* 2021;**28**:28.
49. Cheng K, Rai P, Plagov A, Lan XQ, Kumar D, Salhan D, et al. Transplantation of bone marrow-derived MSCs improves cisplatinum-induced renal injury through paracrine mechanisms. *Exp Mol Pathol* 2013;**94**:466−73.
50. Zeng LT, Yu GP, Yang KL, Xiang W, Li J, Chen H. Efficacy and safety of mesenchymal stem cell transplantation in the treatment of autoimmune diseases (rheumatoid arthritis, systemic lupus erythematosus, inflammatory bowel disease, multiple sclerosis, and ankylosing spondylitis): a systematic review and meta-analysis of randomized controlled trial. *Stem Cells Int* 2022;**2022**:9463314.
51. Li T, Luo CX, Zhang JS, Wei L, Sun W, Xie Q, et al. Efficacy and safety of mesenchymal stem cells co-infusion in allogeneic hematopoietic stem cell transplantation: a systematic review and meta-analysis. *Stem Cell Res Ther* 2021;**12**:246.
52. Lou P, Liu SY, Xu X, Pan C, Lu YR, Liu JP. Extracellular vesicle-based therapeutics for the regeneration of chronic wounds: current knowledge and future perspectives. *Acta Biomater* 2021;**119**:42−56.
53. Le B, Cressman A, Morales D, Fierro FA. First clinical experiences using preconditioning approaches to improve MSC-based therapies. *Curr Stem Cell Rep* 2024;**10**:1−7.